Benefits and Limitations of Unsupported and Supported IrO_x Nanoparticles for the Acidic Oxygen Evolution Reaction

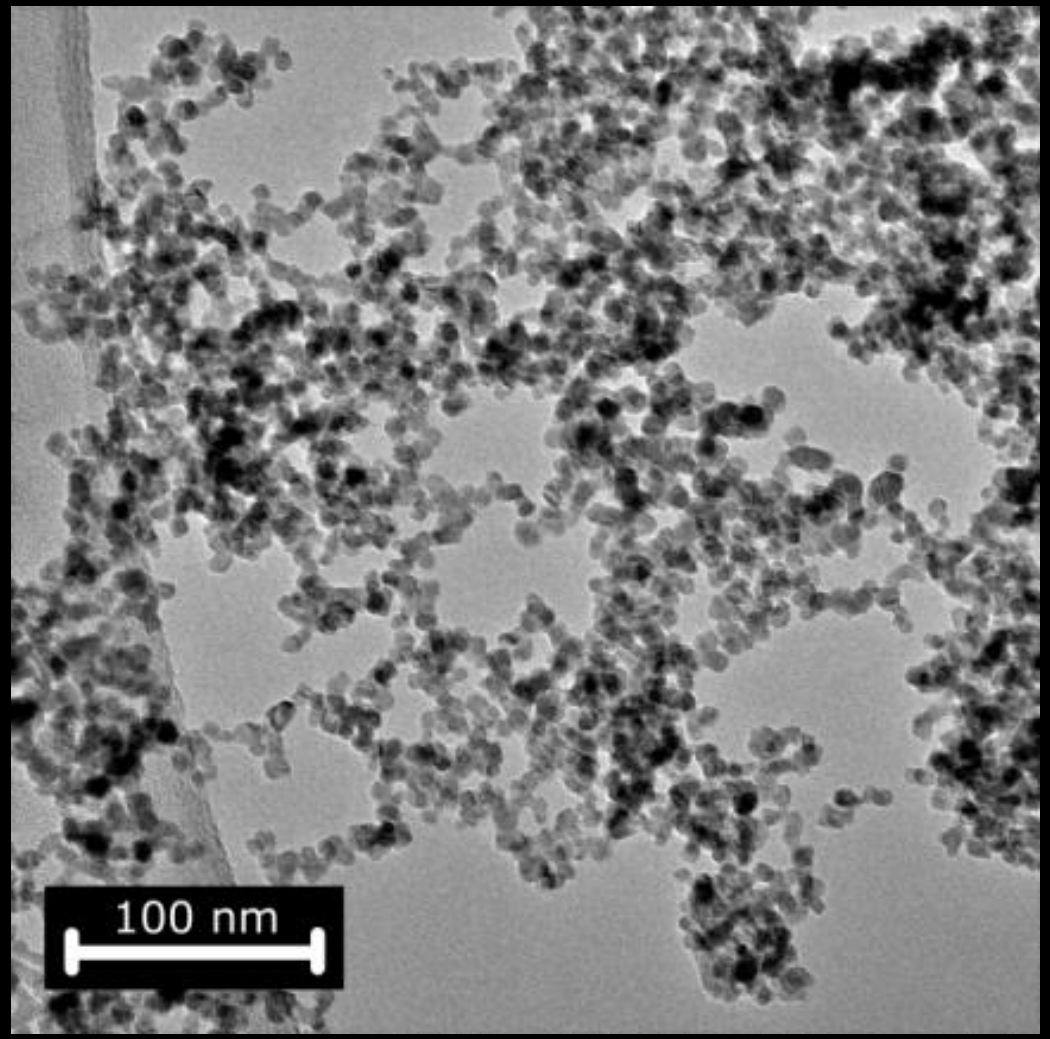

Camila Daiane Ferreira da Silva [1,2], Fabien Claudel [1], Marion Scohy, [1] Sofyane Abbou [1], Raphaël Chattot [1], Vincent Martin [1], Bruno Gilles, [3] Laetitia Dubau [1], Frédéric Maillard [1]

[1] Univ. Grenoble Alpes, Univ. Savoie Mont Blanc, CNRS, Grenoble INP, LEPMI,
38000 Grenoble, France
[2] São Carlos Institute of Chemistry, University of São Paulo, Av. Trabalhador Saocarlense, 400, São Carlos, SP, Brazil
[3] Univ. Grenoble Alpes, CNRS, Grenoble INP, SIMAP, 38000 Grenoble, France

Symposium on the Future of Chemical Energy Conversion –
The Role of Catalysis in Future Energy Systems: From Molecules to Systems – June 13-14, 2022 | Düsseldorf, Germany

Acknowledgements







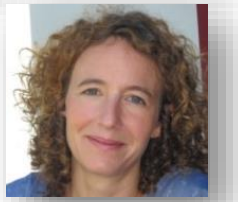

Camila Daiane Ferreira da Silva, Fabien Claudel, Marion Scohy, Raphaël Chattot, Sofyane Abbou, Vincent Martin and Laetitia Dubau.

Bruno Gilles.

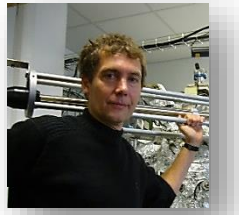

Funding

Alkaline *vs*. acidic water electrolysis

Alkaline WE

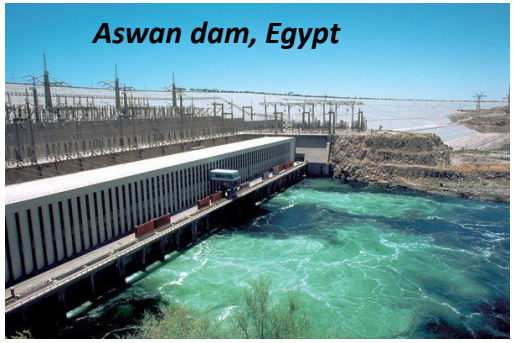

Source: KIMA (Egypt)
165 MW, 37,000 $m^3\ h^{-1}$ of H_2 used in fertilizer industry

❑ Pros

- ❑ Commercialized
- ❑ Abundant non-PGM catalysts (cost & availability)
- ❑ Durability: long-term
- ❑ Stacks: MW range
- ❑ Reliability

❑ Cons

- ❑ Current density: low
- ❑ Low operational pressure
- ❑ Degree of purity: low (crossover)
- ❑ Electrolyte: corrosive
- ❑ Start/stop conditions (intermittency)

PEMWE

Source: Proton On site:
M Series PEM water electrolyzers,
100-400 $m^3\ h^{-1}$ of H_2

❑ Pros

- ❑ Current density: high
- ❑ Can be operated at high pressure (EC compression)
- ❑ Degree of purity: high
- ❑ Quick start/stops (intermittency)
- ❑ Efficiency: 70-80 %

❑ Cons

- ❑ On-going commercialization
- ❑ PGM catalysts (cost & availability)
- ❑ Durability: depends on the operating point and material
- ❑ Membrane electrolyte

[1] M. M. Rashid, M. K. Al Mesfer, H. Naseem, M. Danish, *Int. J. Eng. Adv. Technol*., **2015**, *4*, 80-93.
[2] M. Carmo, D. L. Fritz, J. Mergel, D. Stolten, *Int. J. Hydrogen Energy*, **2013**, *38*, 4901-4934.

OER electrocatalysts

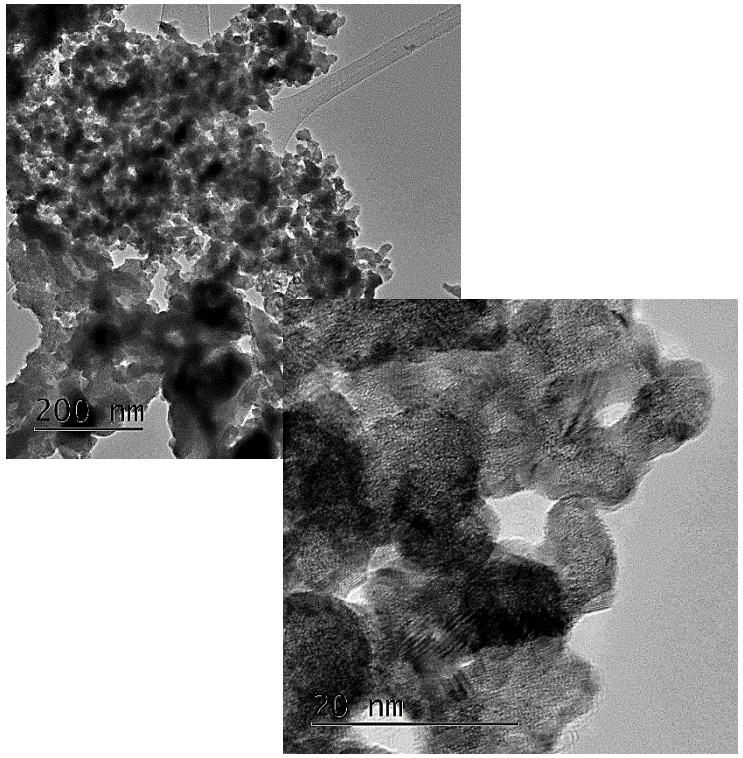

- **OER activity: Ru > Ir > Pd > Rh > Pt > Au > Nb** [1-3].
- **Stability in acidic OER conditions : Ir >> Ru** (RuO_2 corrodes in RuO_4) [4-5].
- Unsupported micrometer-sized IrO_x particles used as OER catalyst in PEMWE

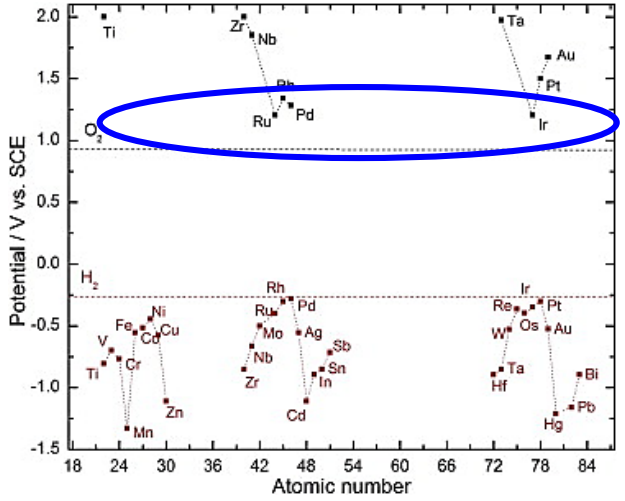

Potential at which the current density attains 2 mA cm^{-2} in 0.1M H_2SO_4, 80 °C.

[1] M. H. Miles, M. A. Thomason, *J. Electrochem. Soc.,* **1976**, *123*, 1459-1461.
[2] I.C. Man, H. Y. Su, F. Calle-Vallejo, H. A. Hansen, J. I. Martínez, N. G. Inoglu, J. Kitchin, T. F. Jaramillo, J. K. Nørskov, J. Rossmeisl, *ChemCatChem*, **2011***, 3,* 1159-1165.
[3] M. Carmo, D. L. Fritz, J. Mergel, D. Stolten, *Int. J. Hydrogen Energy*, **2013**, *38*, 4901-4934.
[4] C. Iwakura, K. Hirao, H. Tamura, *Electrochimica Acta*, **1977**, 22 (4), 329-334.
[5] P. Millet, R. Ngameni, S. A. Grigoriev, N. Mbemba, F. Brisset, A. Ranjbari, C. Etiévant, *Int. J. Hydrogen Energy,* **2010**, *35*, 5043-5052.

Typical Pt/Ir loadings in PEM water electrolyzers

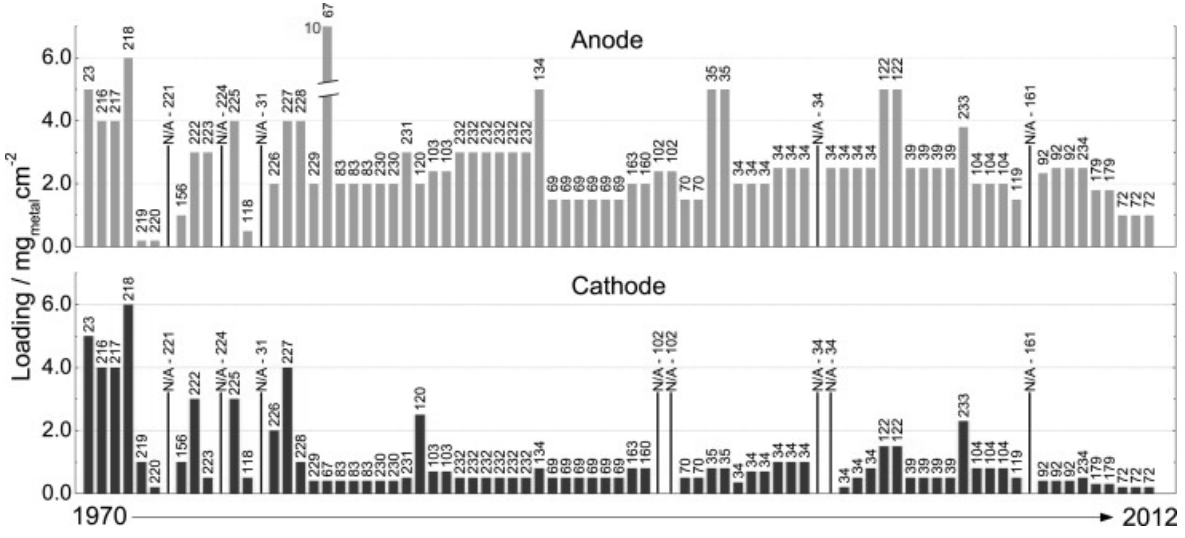

Catalyst loadings (anode and cathode) for typical PEMWE experiments.

- 2013: Typical cathode loadings were ranging between 0.5 and 1.0 mg_{Pt} cm^{-2} [1].
- **2018: Pt loading can be reduced to 0.025 mg_{Pt} cm^{-2}** without any adverse effect on performance [2].
- 2013: Typical anode loadings were ranging between 2.0 and 4.0 mg_{Ir} cm^{-2}.
- **2022: Ir loading can be reduced to 1 mg_{Ir} cm^{-2}**

[1] M. Carmo, D. L. Fritz, J. Mergel, D. Stolten, *Int. J. Hydrogen Energy*, **2013**, *38*, 4901-4934.
[2] M. Bernt, A. Siebel, H.A. Gasteiger, *J. Electrochem. Soc.*, **2018**, 165, F305−F314.

Effect of IrO_2 loading on PEMWE performance

- Thin anodes (< 2 µm, Ir loading < 0.5 mg_{Ir} cm^{-2}), the PEMWE performance decreases (non-contiguous character of the thin catalyst layer).

- Thick electrodes (>10 µm, Ir loading >2 mgIr cm^{-2}), increase of cell voltage and HFR at high current densities, which is attributed to the high water transport resistance through the thick catalyst layer.

- **Best performance in systems obtained for Ir loading ≈1 mg_{Ir} cm^{-2}**, which corresponds to an anode electrode thickness of ≈ 4 µm.

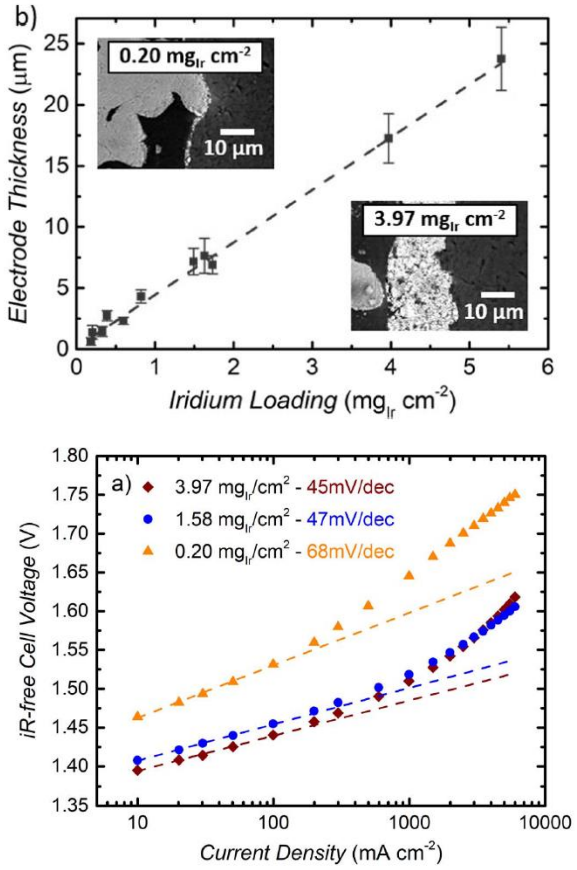

[1] C. Rozain, E. Mayousse, N. Guillet, P. Millet, *Applied Catal. B: Environmental*, **2016**, *182*, 153–160.
[2] M. Bernt, A. Siebel, H. A. Gasteiger, *J. Electrochem. Soc.*, **2018**, *165*, F305-F314.

The oxidation state of Ir atoms influences the long-term OER performance

- Negative degradation rate for Ir(0) : -26 μV h^{-1},
- Positive degradation rate for Ir(IV): + 10 μV h^{-1},
- *U*cell variation flattens with time in both cases,
- **Changes in PEMWE performance related to changes in Ir oxidation state.**

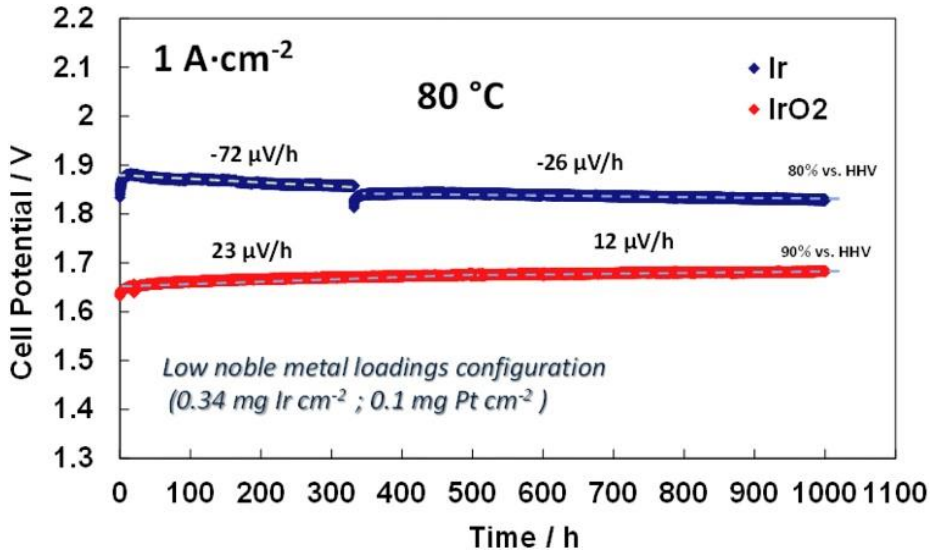

Durability tests at 1 A cm^{-2} and 80°C for two different Ir-black and IrO_2 catalysts-based MEAs.

[1] S. Siracusano, V. Baglio, S. A. Grigoriev, L. Merlo, V. N. Fateev, A. S. Aricò, *J. Power Sources* **2017**, *366*, 105-114.

Outline

- **Insights into the early stages of surface oxidation on well-defined Ir(hkl) single crystals using X-ray photoelectron spectroscopy and inductively-coupled plasma mass spectrometry**

- **Towards a reduction of the Ir loading in PEMWE's anodes**
  - Which supports for IrO_x nanocatalysts?
  - Structure-activity-stability relationships

Conclusions

Ir(hkl) model surfaces

Ir(111)

Most densely packed surface

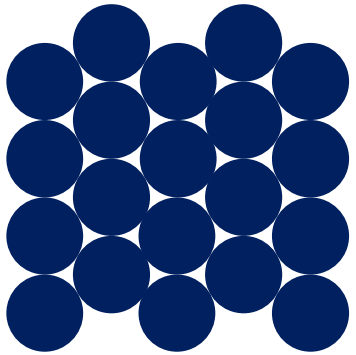

Ir(210)

Open surface

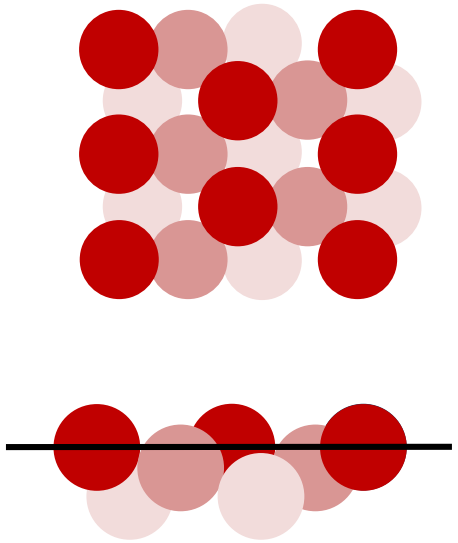

Nanostructured Ir(210)

Reconstructed surface (different cristallographic orientations and presence of surface defects)

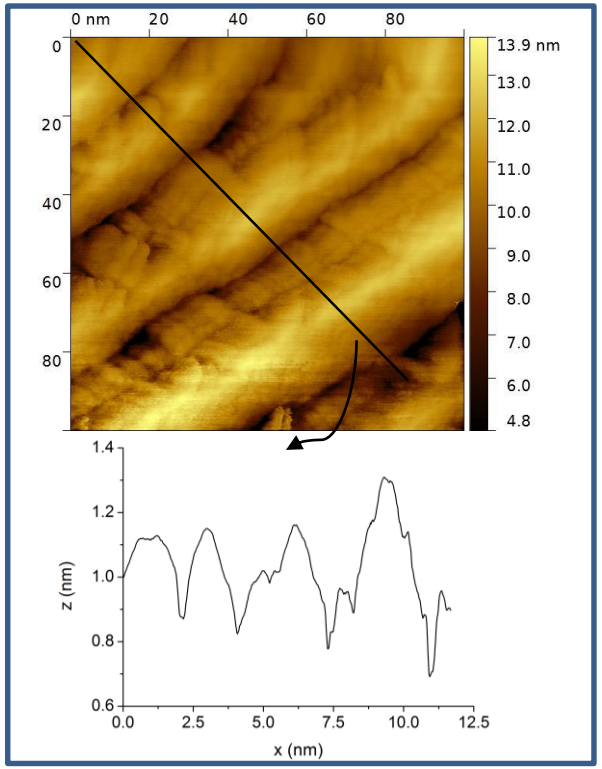

[1] Scohy, M.; Abbou, S.; Martin, V.; Gilles, B.; Sibert, E.; Dubau, L.; Maillard, F., *ACS Catal.* **2019,** *9*, 9859-9869.

Faceting of Ir(210) in O_2 atmosphere

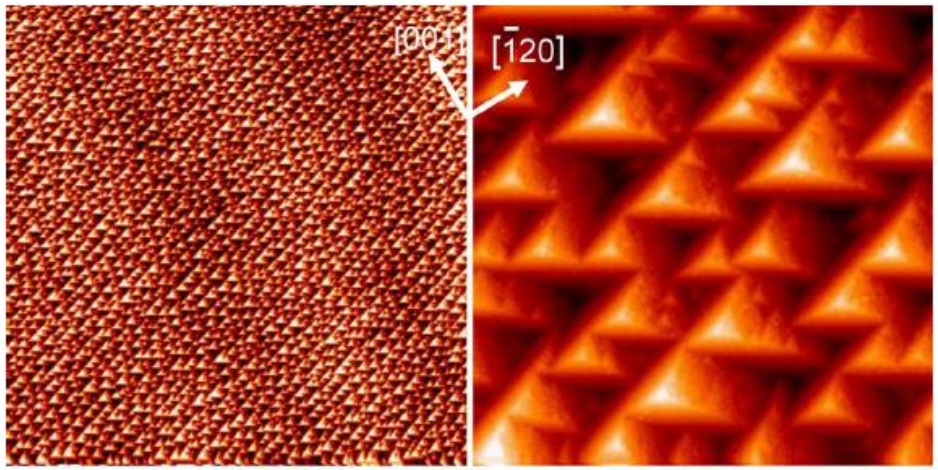

STM images of a fully faceted Ir(210) surface prepared by flash annealing to 1800 K and cooling to room temperature in O_2 atmosphere.

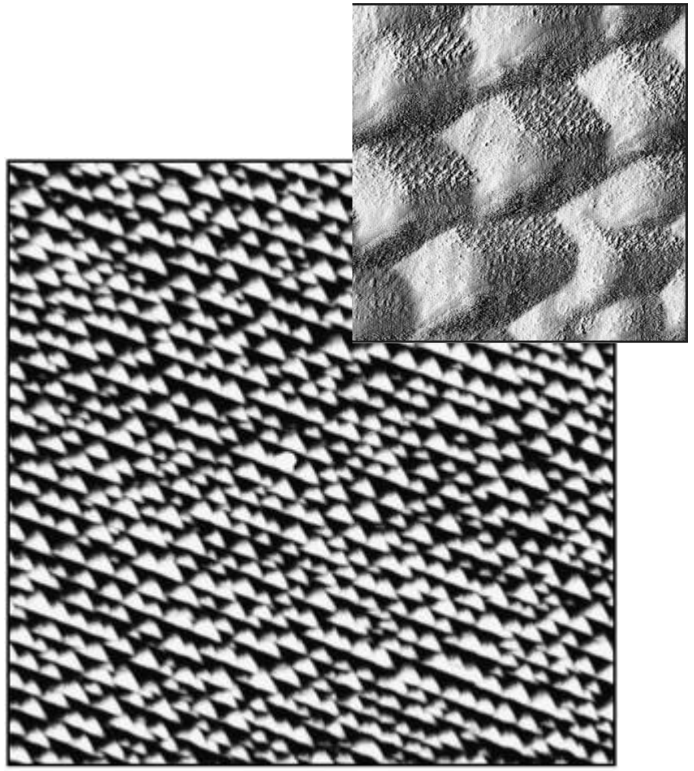

STM-image for nano-faceted Ir(210) in 0.1 M $HClO_4$.

[1] Ermanoski, I.; Pelhos, K.; Chen, W.; Quinton, J. S.; Madey, T. E., *Surf. Sci*. **2004**, *549*, 1-23.
[2] Ermanoski, I.; Kim, C.; Kelty, S. P.; Madey, T. E., *Surf. Sci*. **2005**, *596*, 89-97.
[3] Soliman, K. A.; Simeone, F. C.; Kibler, L. A., *Electrochem. Com*. **2009**, *11*, 31-33.
[4] Kaghazchi, P.; Simeone, F. C.; Soliman, K. A.; Kibler, L. A.; Jacob, T., *Faraday Discuss*. **2008**, *140*, 69-80.

Characterization of the fresh Ir(hkl) surfaces

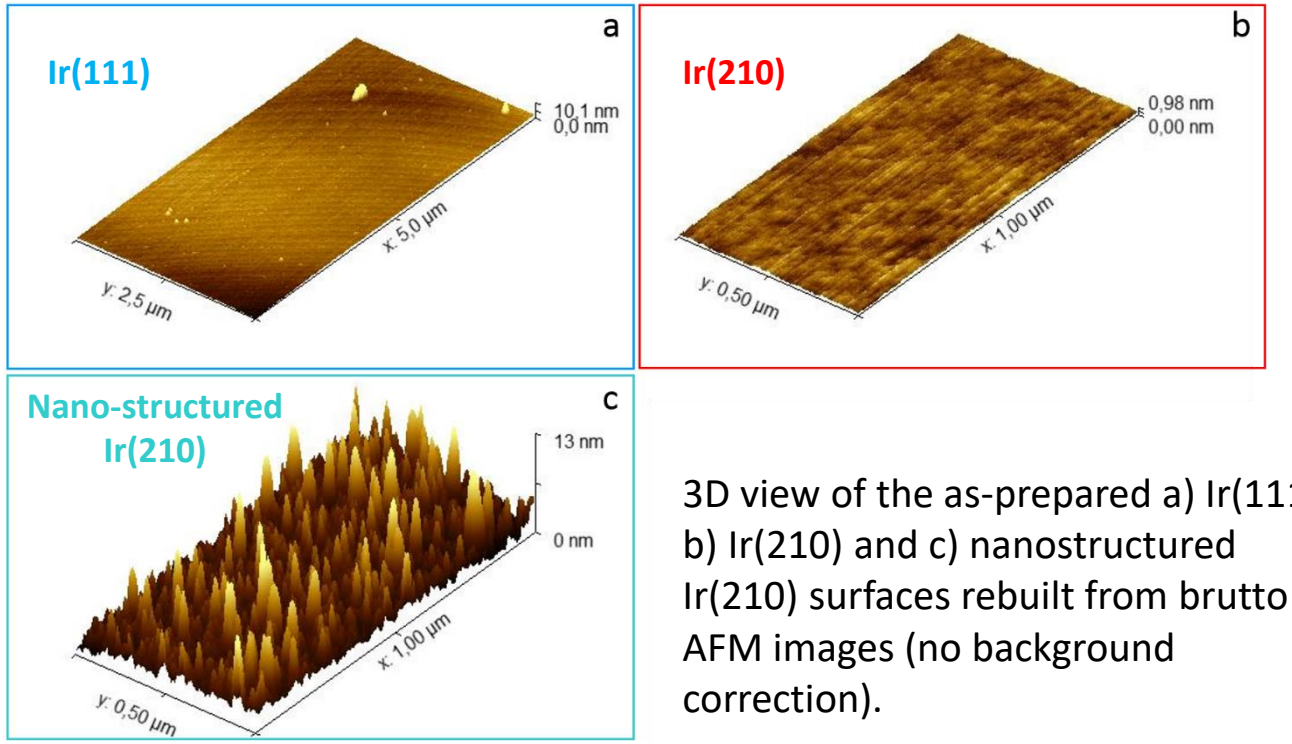

3D view of the as-prepared a) Ir(111), b) Ir(210) and c) nanostructured Ir(210) surfaces rebuilt from brutto AFM images (no background correction).

[1] Scohy, M.; Abbou, S.; Martin, V.; Gilles, B.; Sibert, E.; Dubau, L.; Maillard, F., *ACS Catal.* **2019,** *9*, 9859-9869.

Characterization of the fresh Ir(hkl) surfaces

- CVs agree with literature [1, 2]

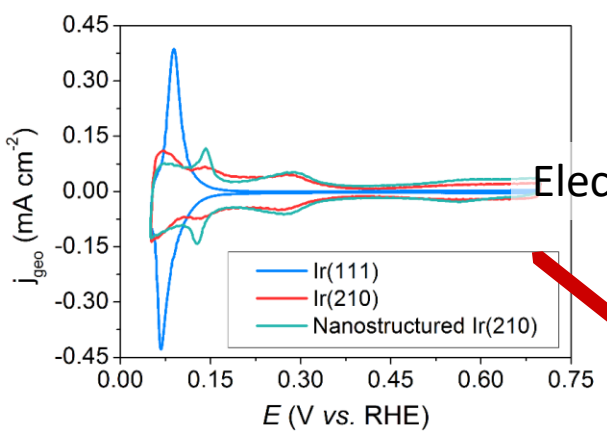

Electrochemistry

As-prepared

Composition

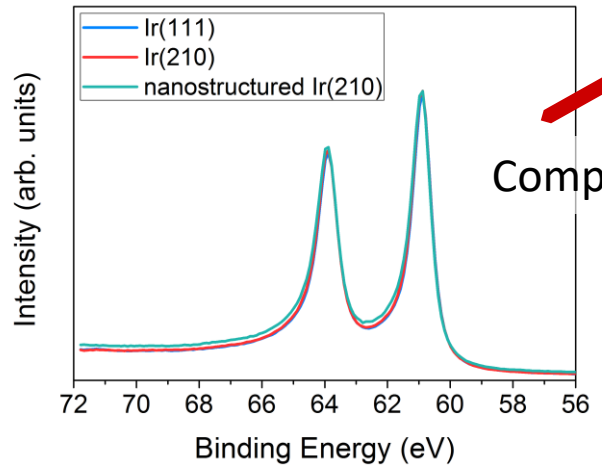

Morphology

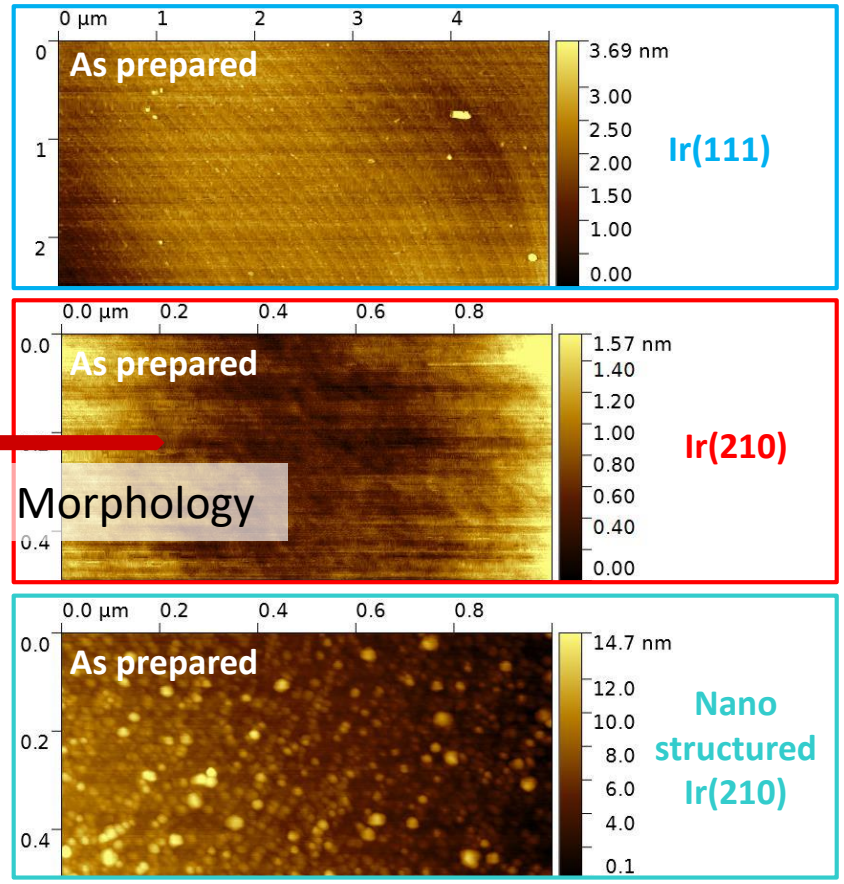

[1] Motoo, S.; Furuya, N., *Electroanal. Chem.* **1984**, *167*, 309-315.

[2] Soliman, K. A.; Kolb, D. M.; Kibler, L. A.; Jacob, T., *Beilstein J. Nanotechnol.* **2014**, *5*, 1349-1356.

After 15 potential cycles between 0.05 V and 1.6 V *vs.* RHE

$$IrO_x(OH)_y + \delta H^+ + \delta e^- \rightleftharpoons IrO_{x-\delta}(OH)_{y+\delta}$$

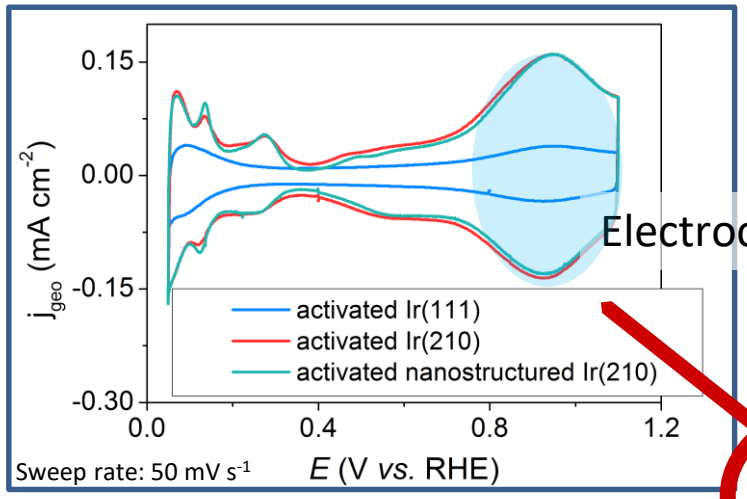

Electrochemistry

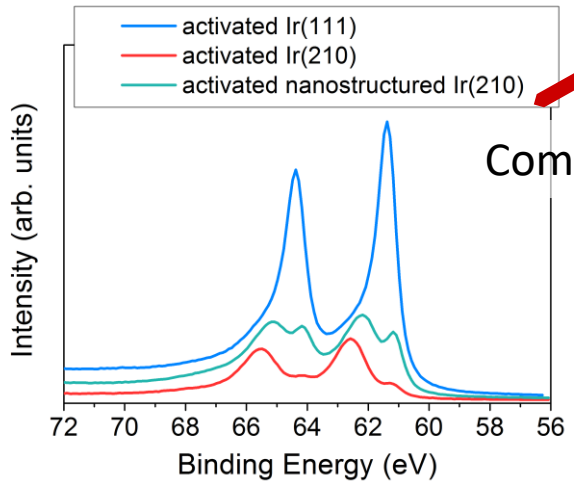

Composition

Conditioned

Morphology

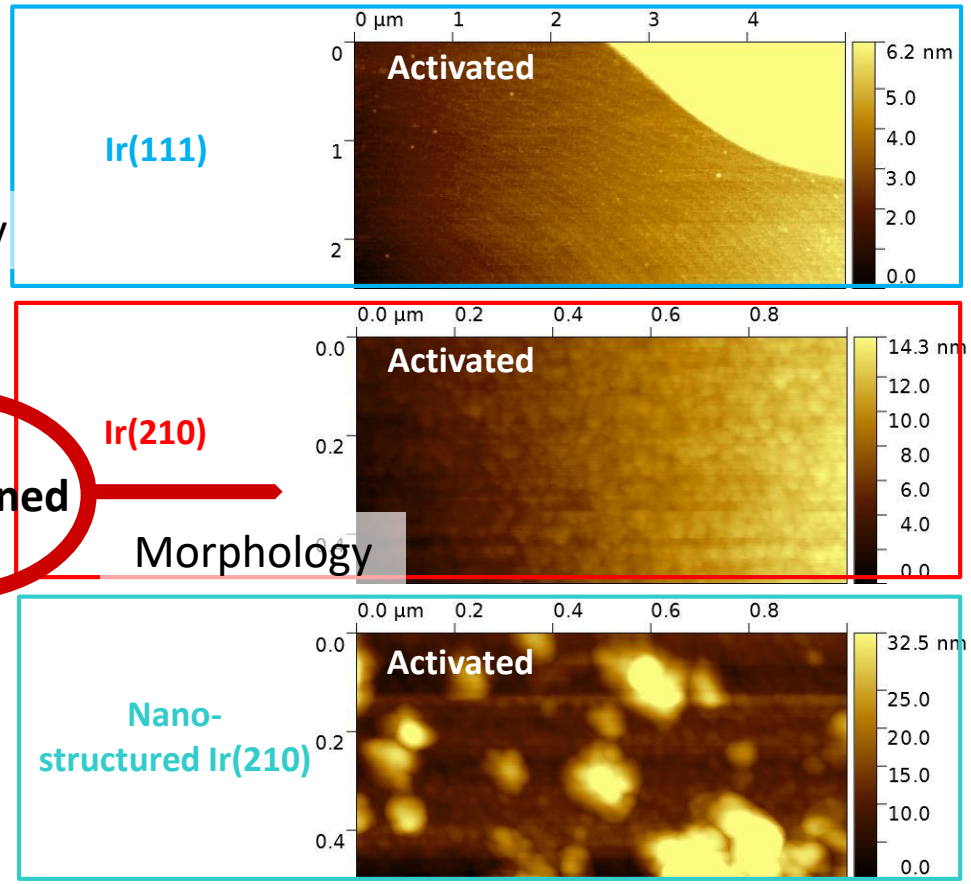

[1] R. Kötz, H, Neff, S. Stucki, J. *Electrochem. Soc.*, **1984**, *131*, 72−77.

[2] Mozota, J.; Conway, B. E, *Electrochim. Acta.* **1983**, *28*, 1-8.

After 15 potential cycles between 0.05 V and 1.6 V *vs.* RHE

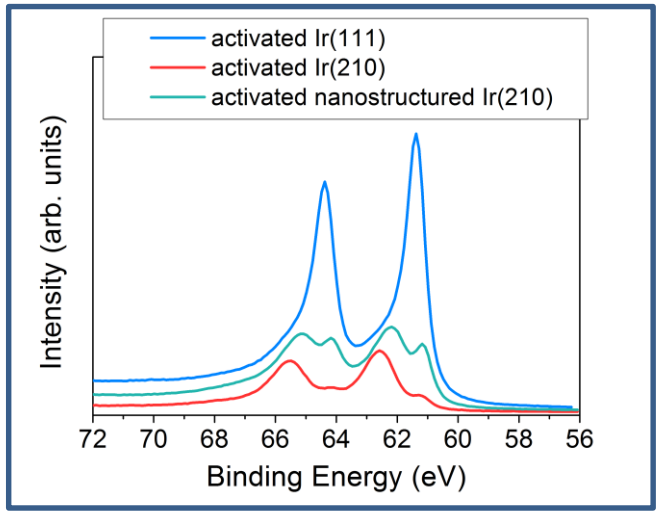

	Ir(0)	Ir(III)	Ir(IV)
Electrochemically-activated Ir(210)	7 %	88 %	5 %
Electrochemically-activated 'nanostructured' Ir(210)	30 %	14 %	56 %
Electrochemically-activated Ir(111)	75 %	0 %	25 %

- Crystallographic orientation-dependent composition of Ir oxides,
- Ir(III) absent from compact Ir(111) surface, predominant on nanostructured Ir(210).

[1] Pfeifer, V.; Jones, T. E.; Velasco Velez, J. J.; Massue, C.; Greiner, M. T.; Arrigo, R.; Teschner, D.; Girgsdies, F.; Scherzer, M.; Allan, J.; Hashagen, M.; Weinberg, G.; Piccinin, S.; Havecker, M.; Knop-Gericke, A.; Schlögl, R., *Phys. Chem. Chem. Phys.* **2016**, *18*, 2292–2296.
[2] Freakley, S. J.; Ruiz-Esquius, J.; Morgan, D. J., *Surf. Interface Anal.* **2017**, *49*, 794–799.

After chronoamperometry at 1.6 V or 1.7 V for 2 h

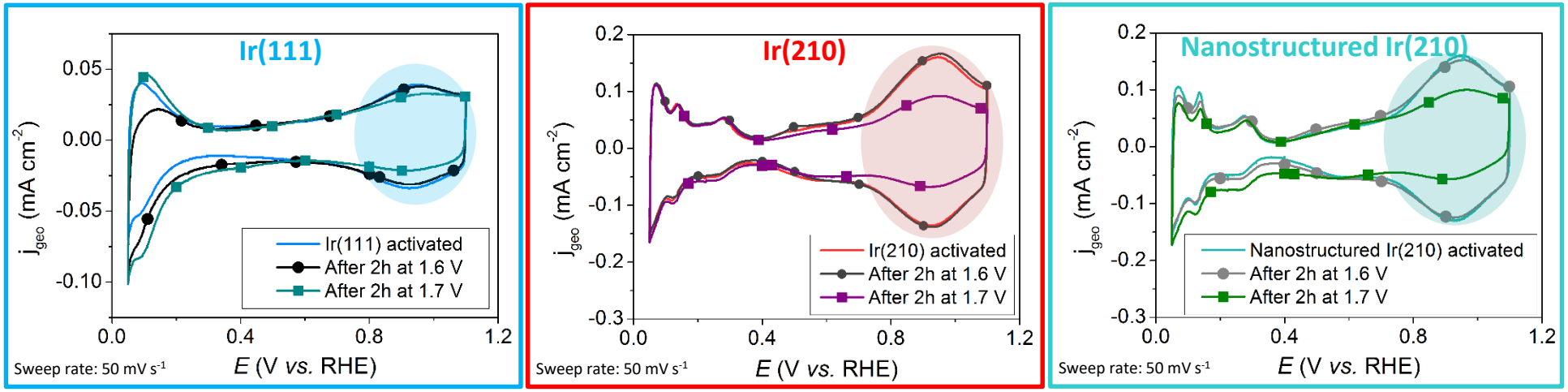

- Drop of the intensity of the peak at 0.9 V, especially after CA at 1.7 V associated with H_{upd} region,
- Decrease in Ir(III) content?

[1] J. Mozota, B. E. Conway, *Electrochim. Acta* **1983**, *28*, 1–8.
[2] Frazer, E. J.; Woods, R., *J. Electroanal. Chem.* **1979**, *102*, 127–130.
[3] B. E. Conway, J. Mozota, *Electrochim. Acta* **1983**, *28*, 9–16.

After chronoamperometry at 1.6 V or 1.7 V for 2 h

		Ir(0)	Ir(III)	Ir(IV)
Ir(210)	Electrochemically activated	7 %	**88 %**	5 %
	After CA at 1.6 V	28 %	**13 %**	59 %
	After CA at 1.7 V	76 %	**2%**	22 %
Ir(111)	Electrochemically activated	75 %	**0 %**	25 %
	After CA at 1.6 V	80 %	**0 %**	20 %
	After CA at 1.7 V	85 %	**0 %**	15 %
Nanostructured Ir(210)	Electrochemically activated	30 %	**14 %**	56 %
	After CA at 1.6 V	35 %	**11 %**	53 %
	After CA at 1.7 V	59 %	**4 %**	37 %

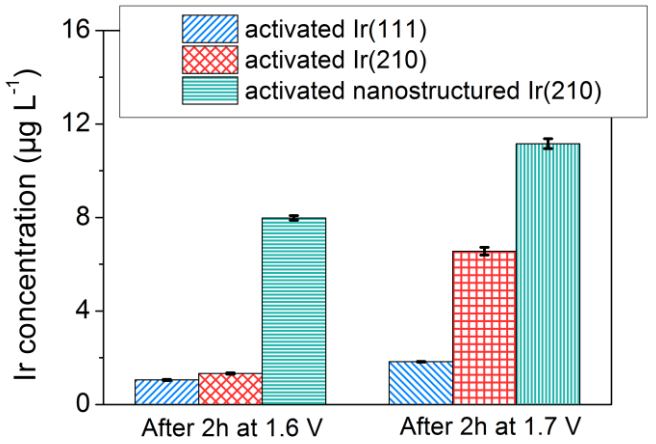

- ❑ Both Ir(III) and Ir(IV) species content decreasing, Ir(0) content increasing.

- ❑ Ir(III) species are dissolving in the electrolyte, [1]
- ❑ Released Ir content increases with increasing concentration of low-coordinated sites.

After chronoamperometry at 1.6 V or 1.7 V for 2 h

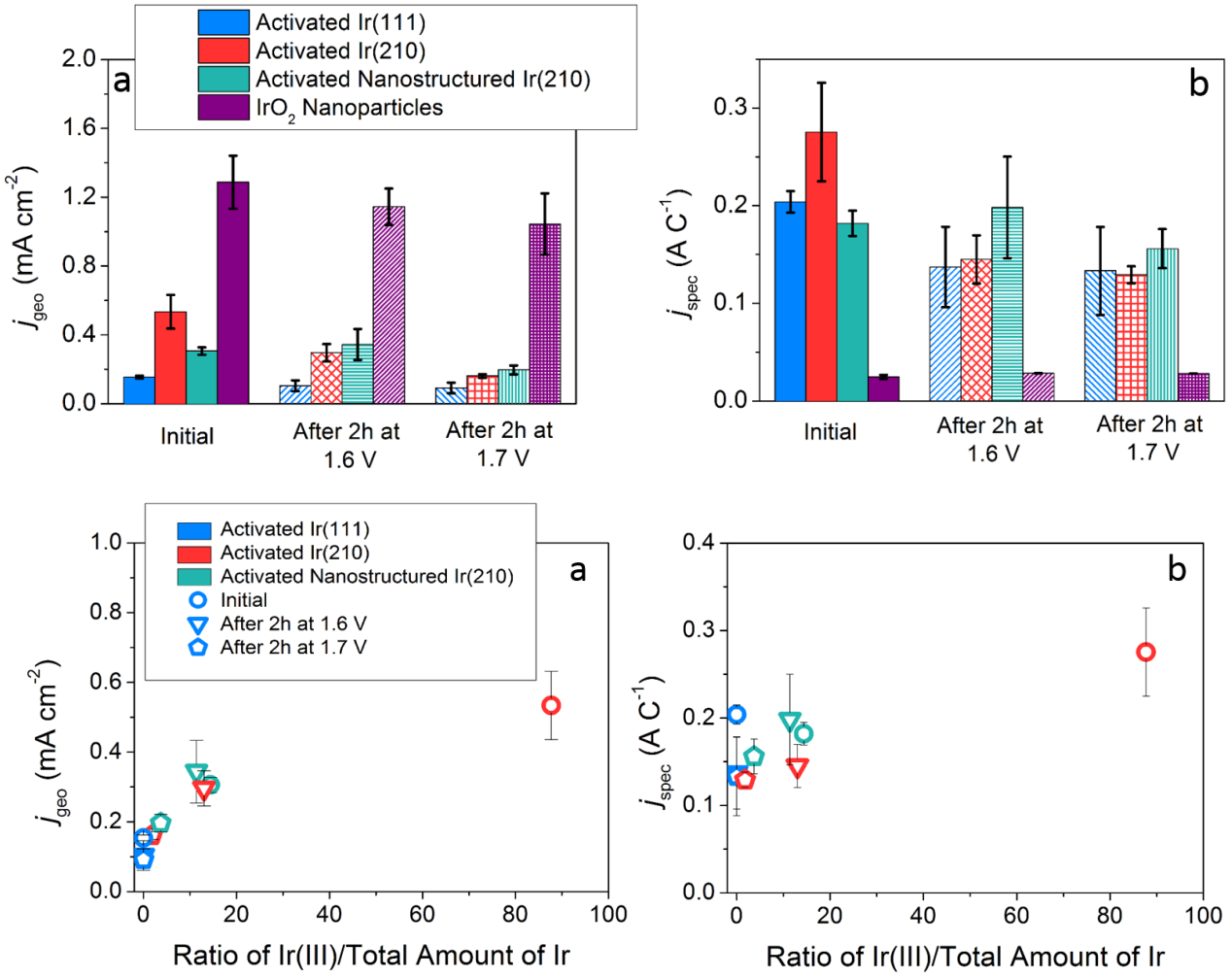

- After chronomaperometry: decrease of the OER activity,
- Same specific activity for the three Ir(hkl) surfaces after 2 hours of polarization at 1.7 V,
- OER specific activity correlates with Ir(III) content determined *ex situ*.

[1] Danilovic, N.; Subbaraman, R.; Chang, K. C.; Chang, S. H.; Kang, Y. J.; Snyder, J.; Paulikas, A. P.; Strmcnik, D.; Kim, Y. T.; Myers, D.; Stamenkovic, V. R.; Markovic, N. M., *J. Phys. Chem. Lett.* **2014**, *5*, 2474–2478.

Ir(III) and O(-I) species correlated?

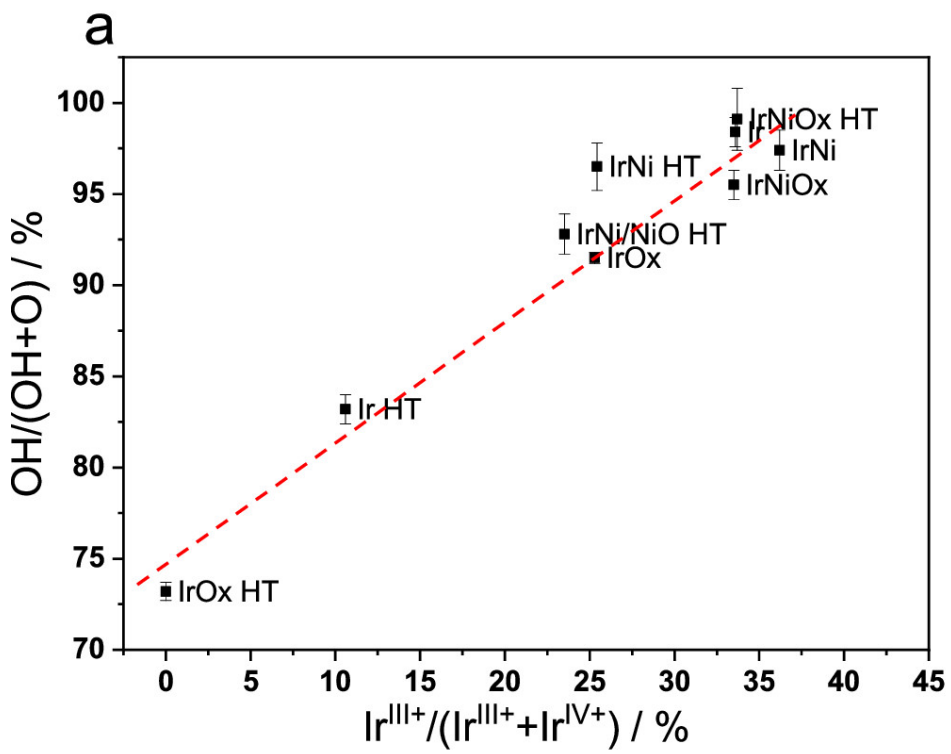

- Electrophilic oxygen O(−I) species shown to be active site towards the OER [1-3]. Similarities with PS II [3].
- Ir leaching from IrO_x lattice → injection of vacancies in the IrO_x shell → number of *d*-band holes on surface Ir increases → increase in the hole character on the O ligands and shorter Ir-O bonds.
- Ir(III) and O(-I) contents correlated [4-6].
- *Ex situ* Ir(III) content was used as a more easily accessible OER activity descriptor.

[1] Pfeifer, V.; Jones, T. E.; Velasco Vélez, J. J.; Massué, C.; Greiner, M. T.; Arrigo, R.; Schlögl, R *et al*., *Phys. Chem. Chem. Phys*. **2016**, *18*, 2292–2296.
[2] Pfeifer, V.; Jones, T. E.; Wrabetz, S.; Massué, C.; Velasco Vélez, J. J.; Arrigo, R.; Schlögl, R. *et al*., *Chem. Sci.* **2016**, *7*, 6791–6795.
[3] Pfeifer, V.; Jones, T. E.; Velasco Vélez, J. J.; Arrigo, R.; Piccinin, S.; Hävecker, M.; Knop-Gericke, A.; Schlögl, R. *Chem. Sci.* **2017**, *8*, 2143–2149.
[4] Nong, H. N.; Reier, T.; Oh, H.-S.; Gliech, M.; Paciok, P.; Vu, T. H. T.; Teschner, D.; Heggen, M.; Petkov, V.; Schlögl, R.; Jones, T.; Strasser, P. *Nature Catalysis* **2018**, *1*, 841−851.
[5] Massué, C.; Pfeifer, V.; van Gastel, M.; Noack, J.; Algara-Siller, G.; Cap, S.; Schlögl, R., *ChemSusChem.* **2017,** *10*, 4786-4798.
[6] Spoeri, C.; Briois, P.; Nong, H. N.; Reier, T.; Billard, A.; Kuehl, S.; Teschner, D.; Strasser, P., *ACS Catal.* **2019,** *9*, 6653-6663.

Activity – Stability – Factor values

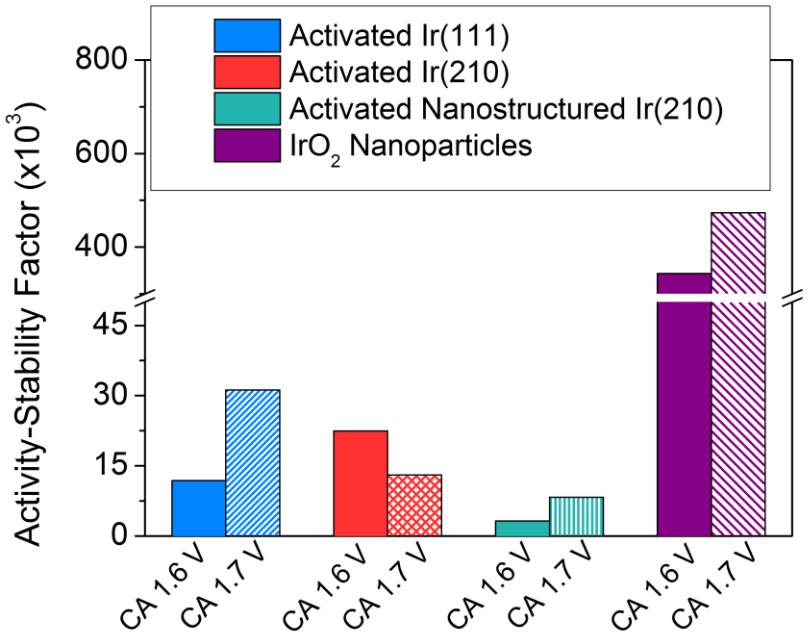

- Potential-dependent ASF [1] values,
- ASF values decrease with increasing concentration of low-coordinated sites,
- Maximal ASF values on IrO_2 particles.

$$\mathrm{ASF} = \left.\frac{J - S}{S}\right|_{\eta}$$

where *J* is the total current density and *S* is the rate of Ir dissolution (equivalent current density calculated from ICP-MS).

[1] Kim, Y. T.; Lopes, P. P.; Park, S. A.; Lee, A. Y.; Lim, J.; Lee, H.; Back, S.; Jung, Y.; Danilovic, N.; Stamenkovic, V.; Erlebacher, J.; Snyder, J.; Markovic, N. M., *Nat. Commun.* **2017,** *8*, 1449.

Intermediate conclusion

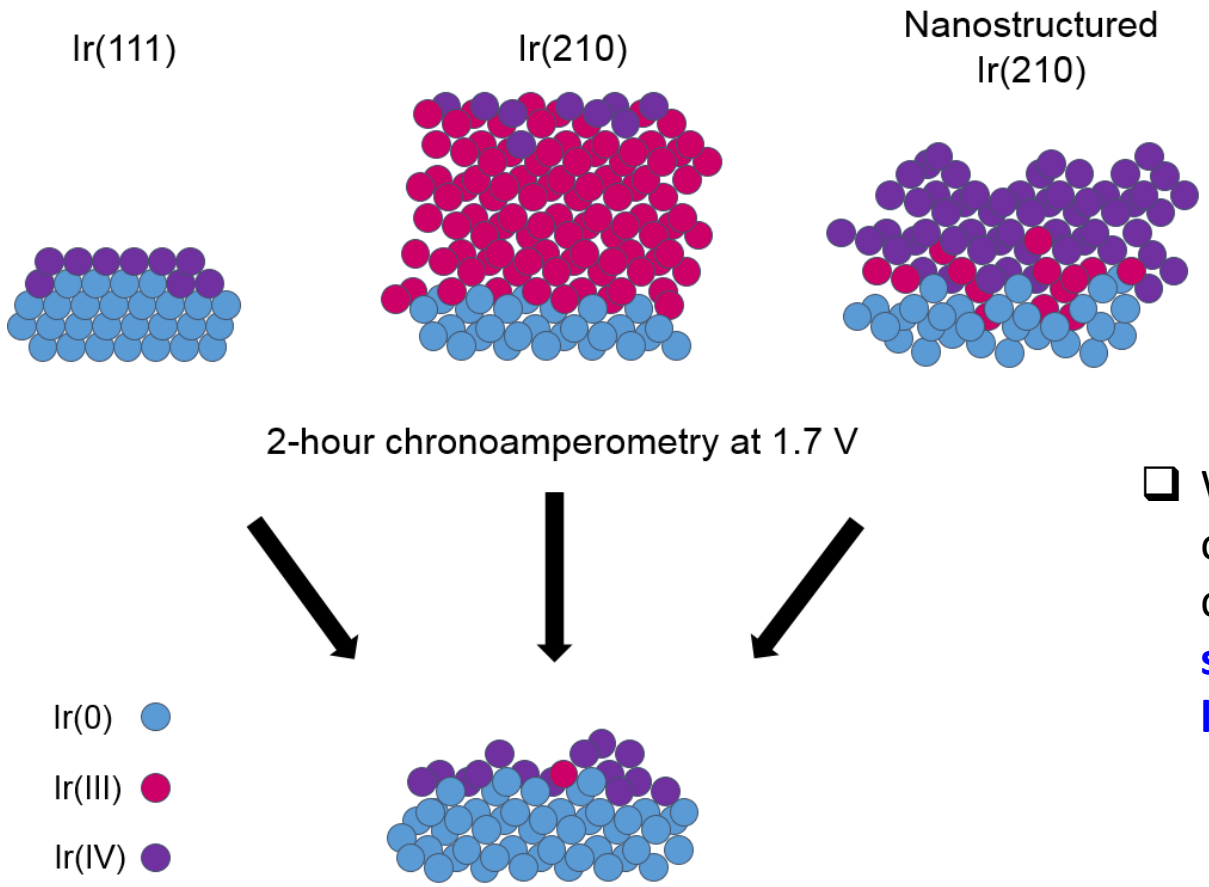

- Whatever the initial crystallographic orientation, proportion of high- and low-coordinated atoms or oxidation state, **Ir single crystal surfaces converge towards a less active yet stable state**.

[1] Scohy, M.; Abbou, S.; Martin, V.; Gilles, B.; Sibert, E.; Dubau, L.; Maillard, F., *ACS Catal.* **2019,** *9*, 9859-9869.

Outline

- **Insights into the early stages of surface oxidation on well-defined Ir(hkl) single crystals using X-ray photoelectron spectroscopy and inductively-coupled plasma mass spectrometry**

- **Towards a reduction of the Ir loading in PEMWE's anodes**
  - Which supports for IrO_x nanocatalysts?
  - Structure-activity-stability relationships

Conclusions

OER electrocatalysts

- **Ir is rare and costly → any alternative?**

- **Mixing IrO_2 with a cheaper "diluent"**: IrO_2 + SnO_2 [1, 2], Ta_2O_5 [3], Nb_2O_5 [4], Sb_2O_5 [5], and their mixtures (*e*.g. SnO_2-IrO_2-Ta_2O_5 [6]) → **unsuccessful** (mostly loss of electron conductivity),

- **Ti@IrO_2 core@shell structure** [7, 8] → beware: TiO_2 layer growths at the interface between the Ti core and the IrO_2 shell,

- **Decrease of the IrO_x crystallite size** [8].

[1] C. P. De Pauli, S. Trasatti, *J. Electroanal. Chem*., **1995**, *396*, 161-168C.
[2] E. Mayousse, F. Maillard, F. Fouda-Onana, O. Sicardy, N. Guillet, *Int. J. Hydrogen Energy,* **2011**, *36*, 10474-10481.
[3] (a) M. Morimitsu, R. Otogawa, M. Matsunaga, *Electrochimica Acta*, **2000**, *46*, 401-406, (b) J. M. Hu, H. M. Meng, J. Q. Zhang, C. N. Cao, *Corr. Sci.* **2002**, *44*, 1655-1668.
[4] A. J. Terezo, J. Bisquert, E. C. Pereira, G. Garcia-Belmonte, *J. Electroanal. Chem*., **2001**, *58*, 59-69.
[5] G. H. Chen, X. M. Chen, P. L. Yue, *J. Phys. Chem. B*, **2002**, *106*, 4364-4369.
[6] S. Ardizzone, C. L. Bianchi, G. Cappelletti, M. Ionita, A. Minguzzi, S. Rondinini, *et al*., *J. Electroanal. Chem*., **2006**, *589*, 160-166.
[7] A. de Oliveira-Sousa, M. A. S. da Silva, S. A. S. Machado, L. A. Avaca, P. de Lima-Neto, *Electrochimica Acta,* **2000**, *45*, 4467-4473.
[8] M. Bernt, C. Schram, J. Schröter, C. Gebauer, J. Byrknes, C. Eickes, H. A. Gasteiger, *J. Electrochem. Soc*., **2021**, *168*, 084513
[8] C. Daiane de Ferreira, F. Claudel, V. Martin, K. Kumar, L. Dubau, F. Maillard *et al*. *ACS Catal.*, **2021***, 11,* 4107-4116.

Building a library of materials

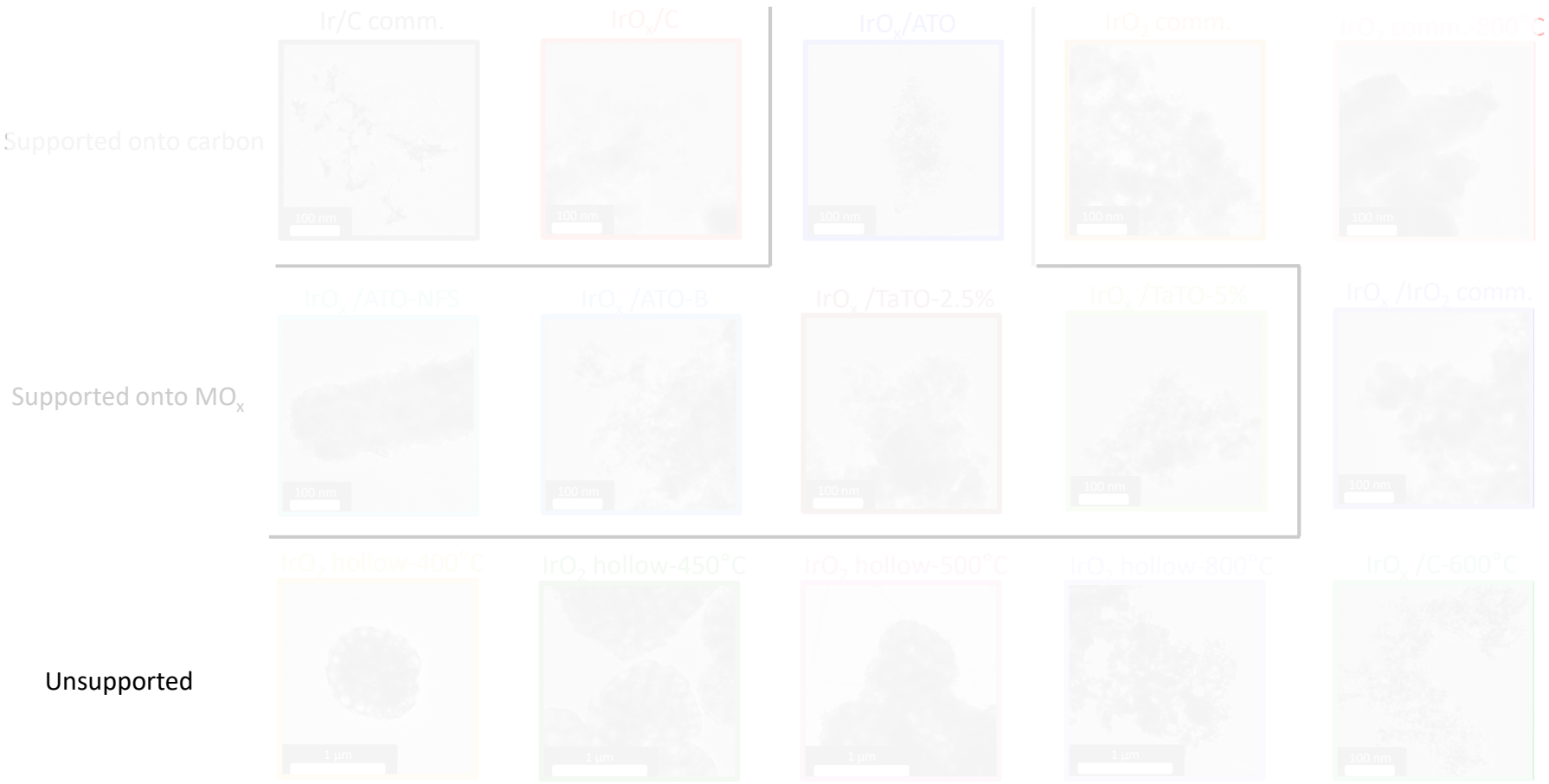

[1] C. Daiane de Ferreira, F. Claudel, V. Martin, R. Chattot, S. Abbou, K. Kumar, I. Jiménez-Morales, S. Cavaliere, D. Jones, J. Rozière, L. Solà-Hernandez, C. Beauger, M. Faustini, J. Peron, B. Gilles, C. Beauger, L. Piccolo, F. H. Barros de Lima, L. Dubau, F. Maillard, *ACS Catal.* **2021**, *11*, 4107-4116.

Electrochemical conditions

❑ H-cell (a P3 glass frit “slows down” redeposition of Ir^{z+} species produced at the WE onto the CE)
- WE: 20 μg_{Ir} cm^{-2} (50 μg_{Ir} cm^{-2} for the unsupported catalysts, except for IrO_2comm. and IrO_x/IrO_2 comm.),
- Separated CE (GC) and WE/Ref. (RHE)
- Ar-saturated 0.05 M H_2SO_4, 25°C.

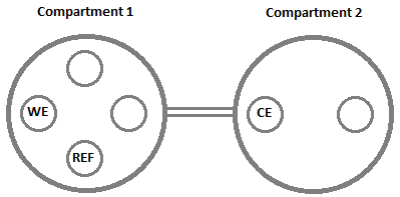

❑ Potentials are corrected with iR drop and reported *vs.* RHE.

❑ Activation: 100 cycles 0.05 – 1.4 V *vs.* RHE, 500 mV s^{-1}, 25°C.

❑ Base voltammograms: 3 cycles 0.05 – 1.4 V *vs.* RHE, 50 mV s^{-1}, 25°C.

❑ OER: LSV from 1.2 to 1.6 V *vs.* RHE, 5 mV s^{-1}, 25°C.

❑Galvanostatic AST: 10 mA cm^{-2} (*ca*. 500 A g^{-1}_{Ir}) and *T* = 80°C

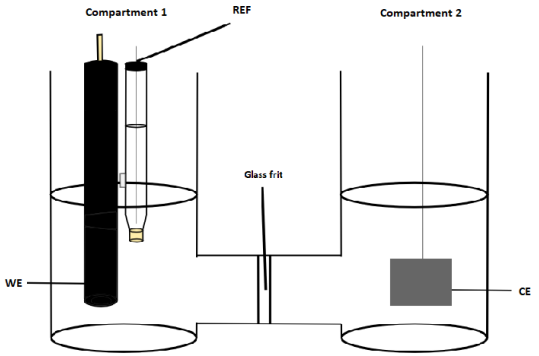

Physical and electrochemical characterization of the catalysts

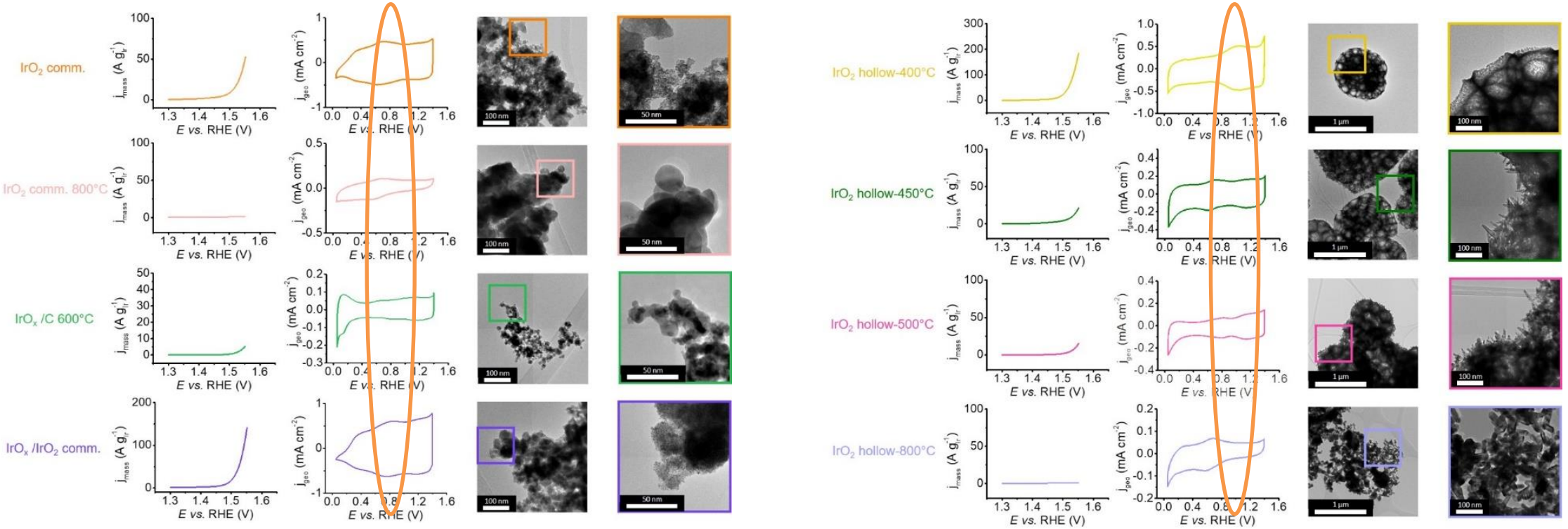

- Amorphous Ir oxyhydroxides produced by polyol route well performing towards the OER [1-3],
- Supported >> unsupported catalysts [4]

[1] S. Gottesfeld, S. Srinivasan, *J. Electroanal. Chem. Interfacial Electrochem.*, **1978**, *86*, 89.
[2] R. Kötz, H, Neff, S. Stucki, J. *Electrochem. Soc.*, **1984**, *131*, 72-77.
[3] T. Reier, D. Teschner, T. Lunkenbein, A. Bergmann, S. Selve, R. Kraehnert, R. Schlögl, P. Strasser, *J. Electrochem. Soc.*, **2014**, *161*, F876−F882
[4] F. Claudel, L. Dubau, G. Berthomé, L. Sola-Hernandez, C. Beauger, L. Piccolo, F. Maillard, *ACS Catal.*, **2019**, *9*, 4688-4698.

Charge-normalized activity towards the OER

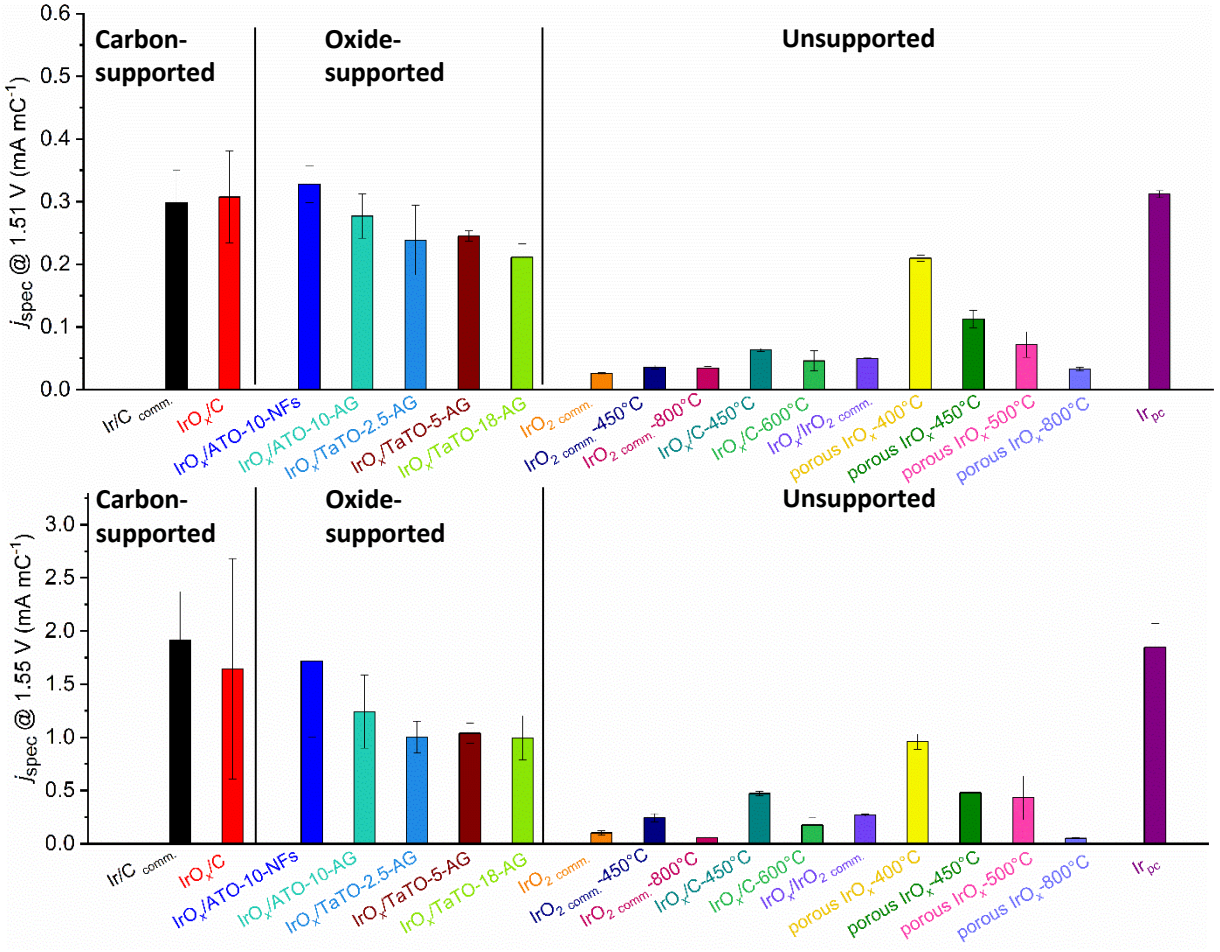

- Amorphous Ir oxyhydroxides best performing towards the OER, in agreement with [1-3].
- **Supported > Unsupported**

[1] T. Reier, D. Teschner, T. Lunkenbein, A. Bergmann, S. Selve, R. Kraehnert, R. Schlögl, P. Strasser, *J. Electrochem. Soc.*, **2014**, *161*, F876–F882.

[2] S. Cherevko, T. Reier, A. R. Zeradjanin, Z. Pawolek, P. Strasser, K. J. J. Mayrhofer, K. J. J., *Electrochem. Com.* **2014**, *48*, 81-85

[3] F. Claudel, L. Dubau, G. Berthomé, L. Sola-Hernandez, C. Beauger, L. Piccolo, F. Maillard, *ACS Catal.*, **2019**, *9*, 4688-4698.

Mass-normalized activity towards the OER

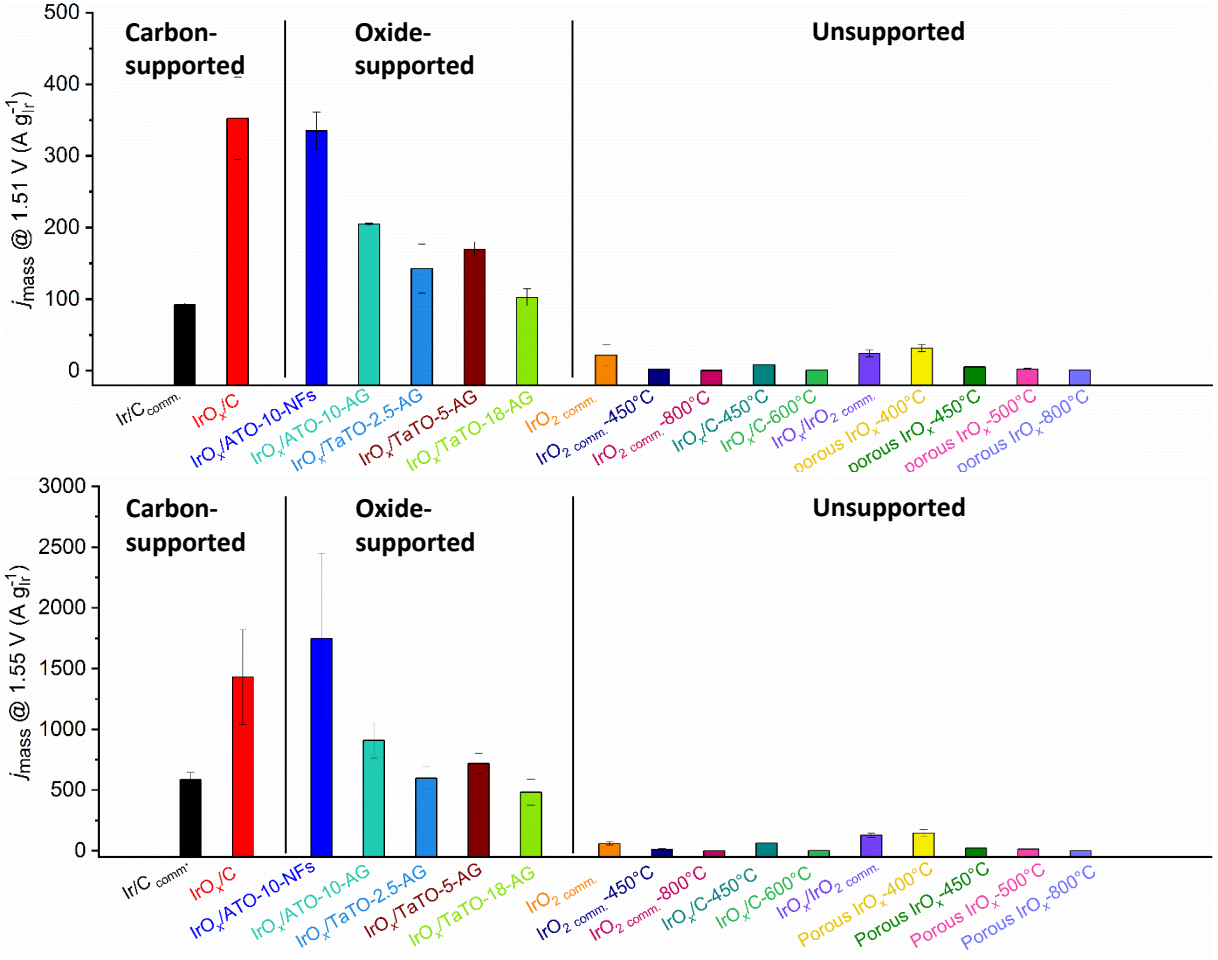

❑ **Supported > Unsupported**

❑ **MA = ASD x TOF x *F*/*N*a** [1]

- With MA, the OER mass activity (A g^{-1} powder),
- ASD, the active site density (site g^{-1} powder),
- TOF, the turnover frequency (electrons $site^{-1}$ s^{-1}),
- *F* the Faraday's constant (A s mol^{-1}),
- *N*a Avogadro's number (electrons mol^{-1})

❑ Reasons are combined effects of mixed Ir oxidation states, small crystallites and high ASD values

[1] Gasteiger, H. A.; Kocha, S. S.; Sompalli, B.; Wagner, F. T., *Appl. Catal. B.*, **2005,** *56*, 9-35.

Towards *S*-number values

❑ Galvanostatic AST: 10 mA cm^{-2} (*ca*. 500 A g^{-1}_{Ir}) and T = 80°C until cut-off voltage (U = 2V) is reached.

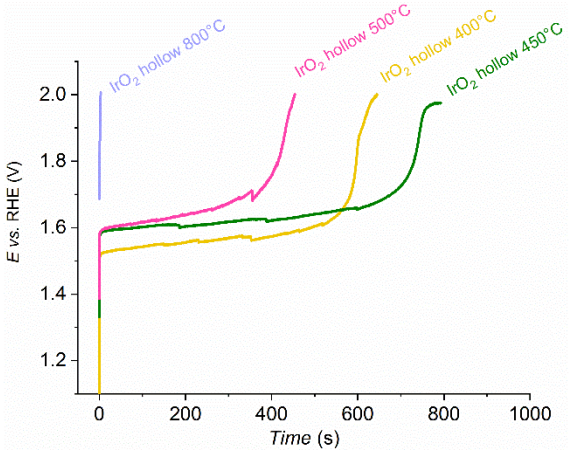

Electrolyte sampling

→

TEM
X-EDS
ICP-MS analysis

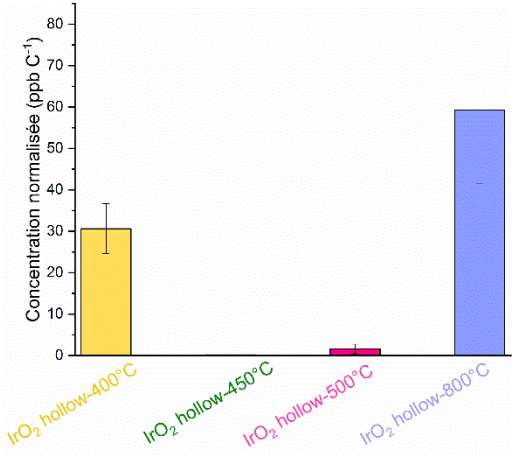

Changes in morphology

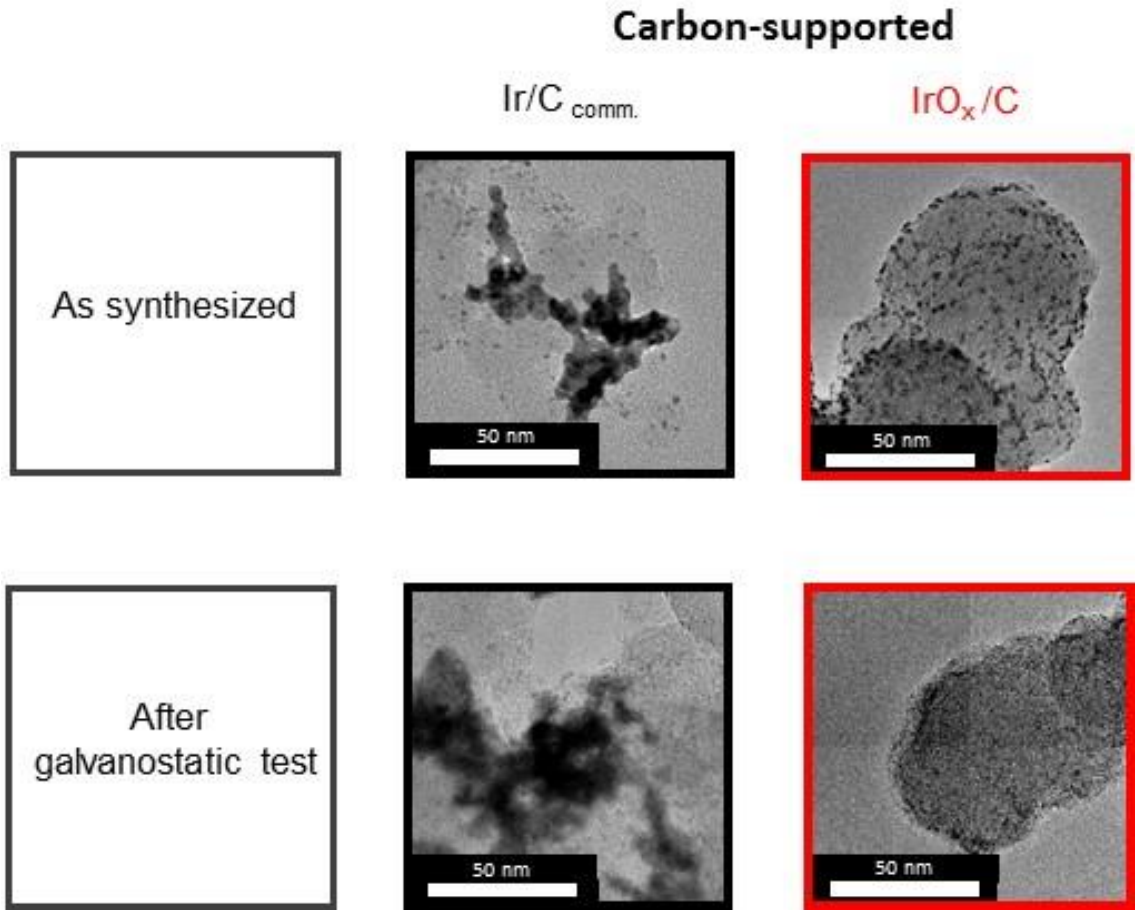

Changes in morphology

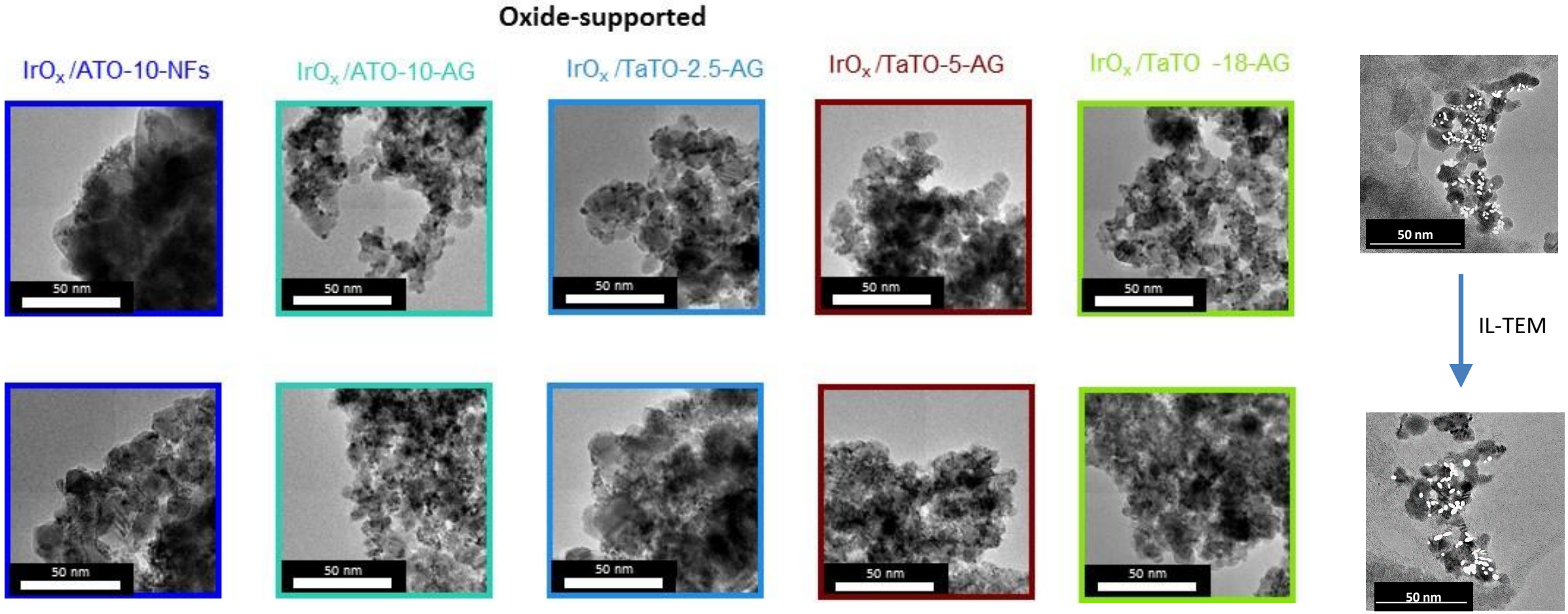

[1] F. Claudel, L. Dubau, G. Berthomé, L. Sola-Hernandez, C. Beauger, L. Piccolo, F. Maillard, *ACS Catal.*, **2019**, *9*, 4688-4698.

Metrics used to compare the durability of OER catalysts

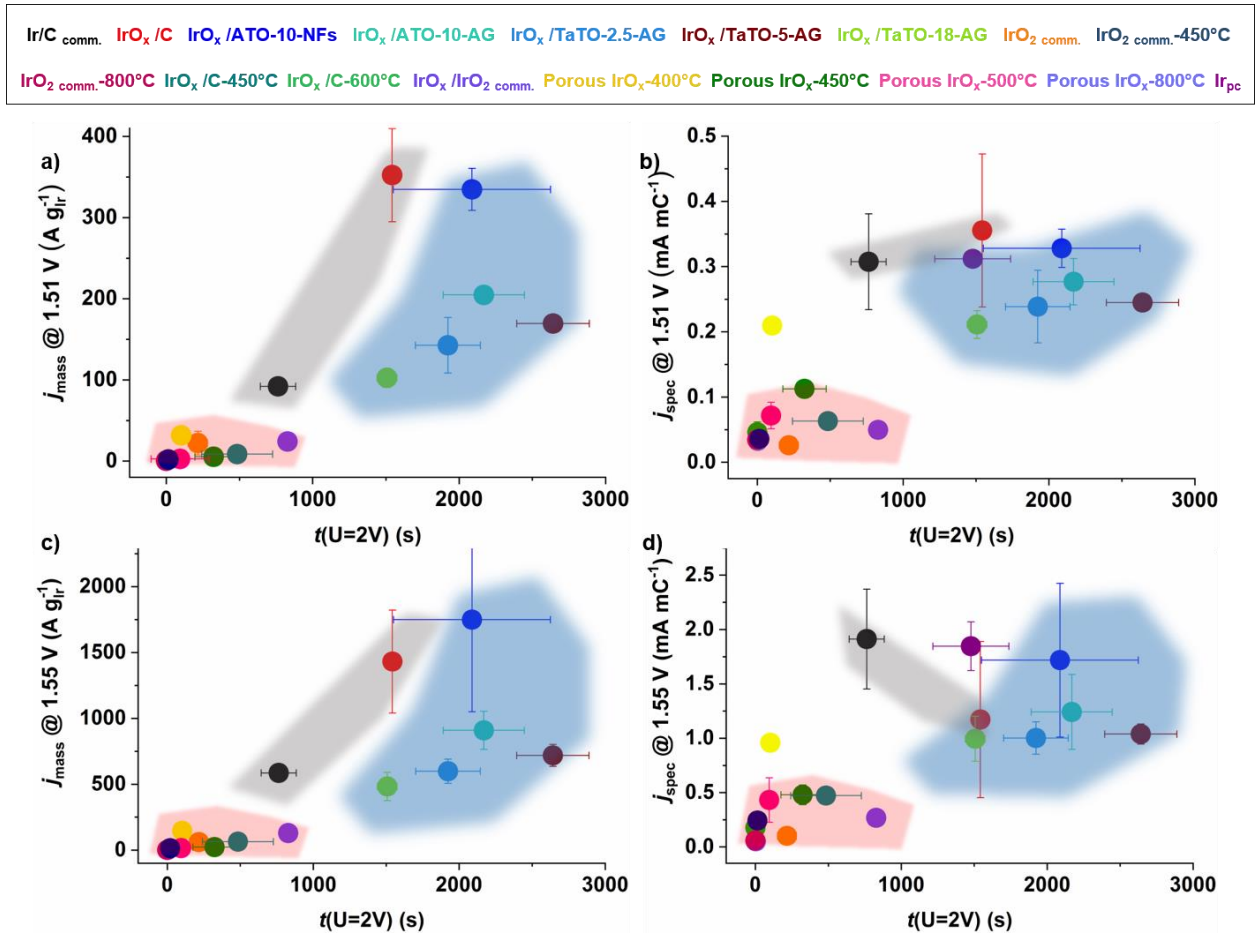

- **Most efficient OER catalysts also seem to be the most durable,**
- Combined effects of TOF and ASD:

  MA = ASD x TOF x *F/N*a implies that the most active catalysts operate at lower potential (less oxidizing conditions)
- The time required to reach cut-off voltage is in fact poorly related to the durability of the catalyst.

Metrics used to compare the durability of OER catalysts

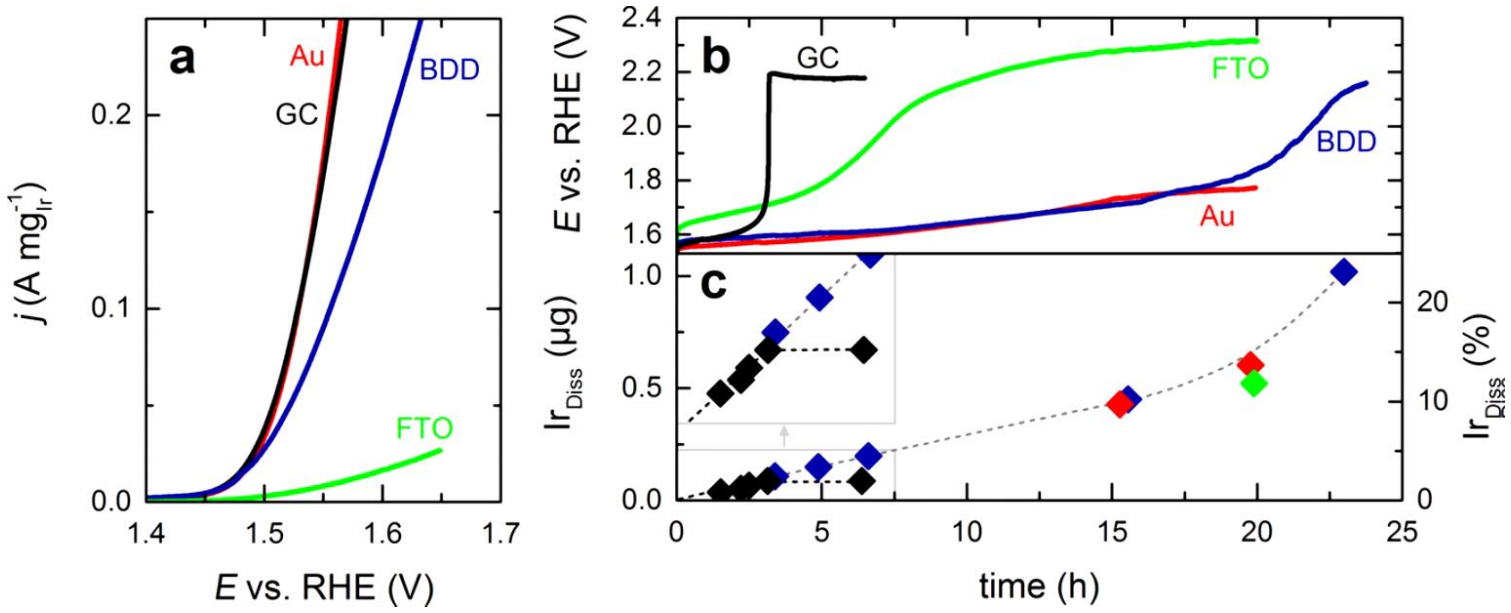

- Passivation of the backing electrode [1]?

[1] Geiger, S.; Kasian, O.; Mingers, A. M.; Nicley, S. S.; Haenen, K.; Mayrhofer, K. J. J.; Cherevko, S., *ChemSusChem*. **2017**, *10*, 4140-4143.

Metrics used to compare the durability of OER catalysts

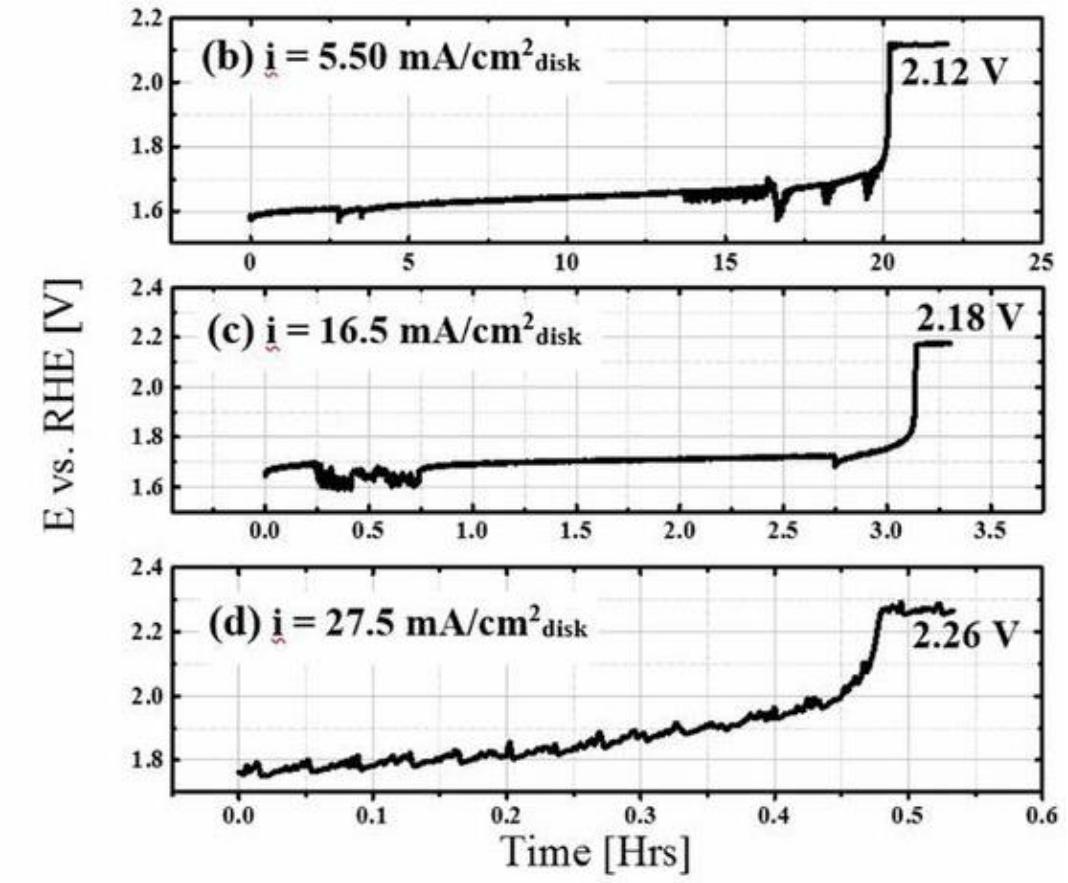

- Passivation of the backing electrode [1]?
- Similar effect observed on Au disk [2].

[1] Geiger, S.; Kasian, O.; Mingers, A. M.; Nicley, S. S.; Haenen, K.; Mayrhofer, K. J. J.; Cherevko, S., ChemSusChem. **2017**, *10*, 4140-4143.
[2] El-Sayed, H. A.; Weiss, A.; Olbrich, L. F.; Putro, G. P.; Gasteiger, H. A., *J. Electrochem. Soc.* **2019,** *166*, F458-F464.

Metrics used to compare the durability of OER catalysts

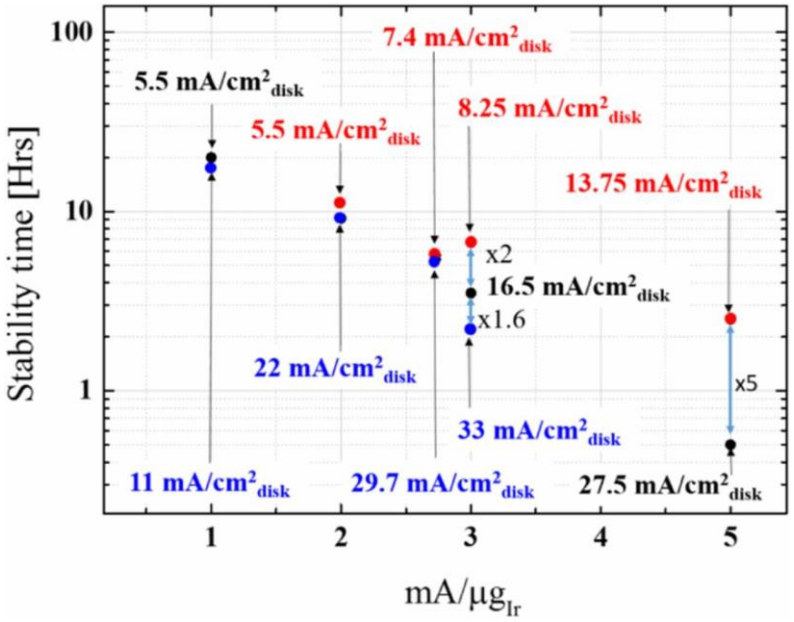

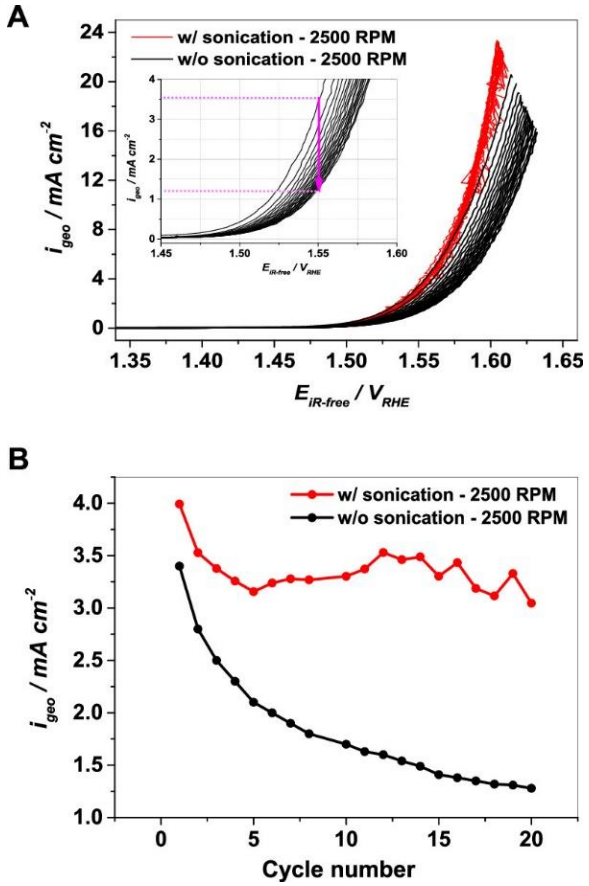

- ❑ Passivation of the backing electrode [1]?
- ❑ Time to reach cut-off voltage is inversely % to current density and to Ir loading [2].
- ❑ **Poisoning by O_2 bubbles in/at the TF electrode**:
  - Time to reach cut-off voltage is inversely % to current density and Ir loading [2].
  - OER activity stable upon sonication, otherwise drops continuously [3]

[1] Geiger, S.; Kasian, O.; Mingers, A. M.; Nicley, S. S.; Haenen, K.; Mayrhofer, K. J. J.; Cherevko, S., *ChemSusChem*. **2017**, *10*, 4140-4143.
[2] El-Sayed, H. A.; Weiss, A.; Olbrich, L. F.; Putro, G. P.; Gasteiger, H. A., *J. Electrochem. Soc.* **2019,** *166*, F458-F464.
[3] Hartig-Weiss, A. Tovini, M. F.; Gasteiger, H. A.; El-Sayed, H. A., *ACS Appl. Energy Mater*. **2020**, *3*, 10323-10327

S-number values [1]

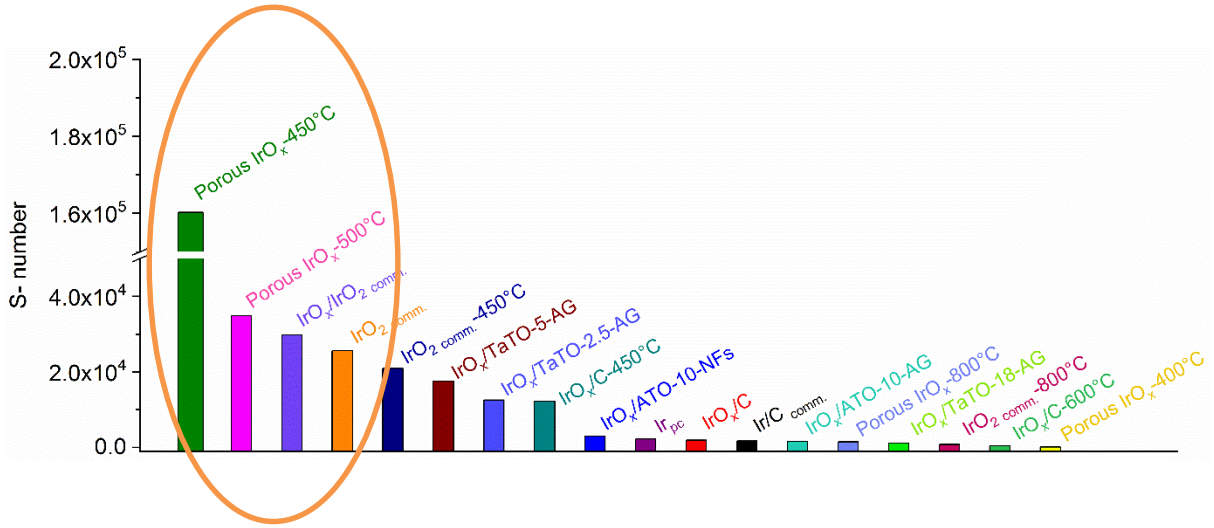

❑ **Unsupported >> Supported**

❑ Porous IrO_x-450°C: 6-fold enhancement of the *S*-number value with respect to reference $IrO_{2\ comm.}$

S-number values calculated for all the electrocatalysts during a galvanostatic AST performed in Ar-saturated 0.05 M H_2SO_4 at j = 10 mA cm^{-2}_{geo}, T = 80 °C, $U_{cut\text{-}off}$ = 2 V *vs.* RHE

$$S - number = \frac{n(O_2)}{n(Ir)} = \frac{i}{i_{\text{dissol}}}$$ [1]

$$n_{O_2} = \frac{1}{zF}\int i\,(t)dt$$

$$n_{Ir} = \frac{[Ir]V}{M_{\text{Ir}}}$$

[1] Geiger, S.; Kasian, O.; Ledendecker, M.; Pizzutilo, E.; Mingers, A. M.; Fu, W. T.; Diaz-Morales, O.; Li, Z.; Oellers, T.; Fruchter, L.; Ludwig, A.; Mayrhofer, K. J. J.; Koper, M. T. M.; Cherevko, S., *Nat. Catal.* **2018,** *1* (7), 508-515.
[2] S. Abbou, R. Chattot, V. Martin, F. Claudel, L. Solà-Hernández, C. Beauger, L. Dubau, F. Maillard, *ACS Catal.*, **2020**, *10*, 7283-7284.

S-number values [1]

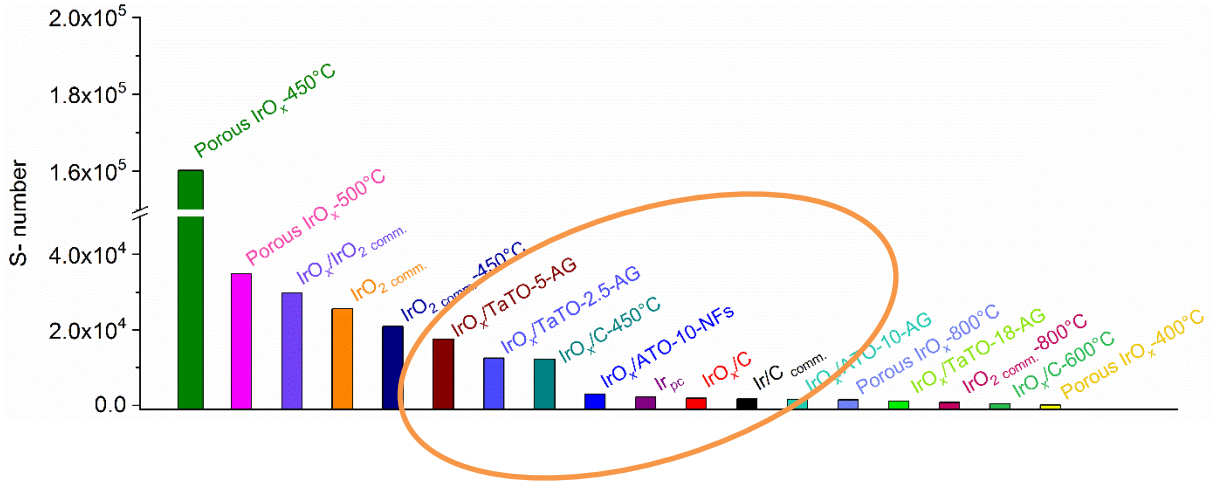

- IrO_x/TaTO, best supported catalyst in terms of *S*-number.
- In agreement with [2].

S-number values calculated for all the electrocatalysts during a galvanostatic AST performed in Ar-saturated 0.05 M H_2SO_4 at j = 10 mA cm^{-2}_{geo}, T = 80 °C, $U_{cut\text{-}off}$ = 2 V *vs.* RHE

$$S - number = \frac{n(O_2)}{n(Ir)} = \frac{i}{i_{dissol}} \text{ [1]}$$

$$n_{O_2} = \frac{1}{zF}\int i\,(t)dt$$

$$n_{Ir} = \frac{[Ir]V}{M_{Ir}}$$

[1] Geiger, S.; Kasian, O.; Ledendecker, M.; Pizzutilo, E.; Mingers, A. M.; Fu, W. T.; Diaz-Morales, O.; Li, Z.; Oellers, T.; Fruchter, L.; Ludwig, A.; Mayrhofer, K. J. J.; Koper, M. T. M.; Cherevko, S., *Nat. Catal.* **2018,** *1* (7), 508-515.
[2] S. Abbou, R. Chattot, V. Martin, F. Claudel, L. Solà-Hernández, C. Beauger, L. Dubau, F. Maillard, *ACS Catal.*, **2020**, *10*, 7283-7284.

Flow cell ICP-MS

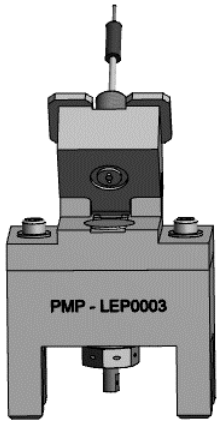

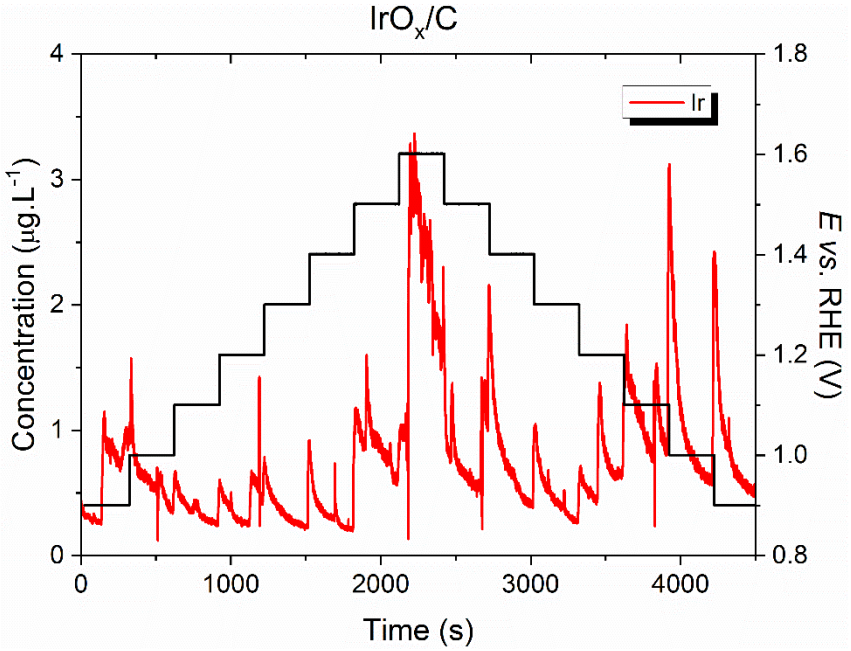

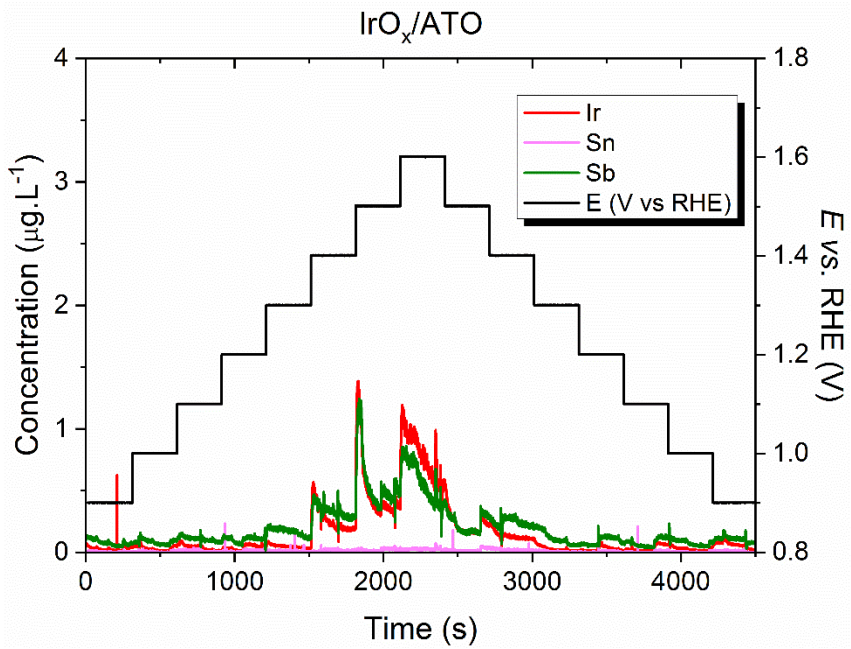

- ATO improves the stability of IrO_x NPs *vs*. Vulcan XC72 but…
- Amount of Ir and Sb being dissolved correlate.

- 20 μg_{Ir} cm^{-2} (100 μg_{Ir} cm^{-2} for IrO_2)
- Ar-saturated 0.05 M H_2SO_4 @ 22 ± 2°C
- 100 mV steps between 0.9 – 1.6 V *vs*. RHE – 300 s each – 25°C)

[1] S. Abbou, R. Chattot, V. Martin, F. Claudel, L. Solà-Hernández, C. Beauger, L. Dubau, F. Maillard, *ACS Catal.*, **2020**, *10*, 7283-7284.

Flow cell ICP-MS

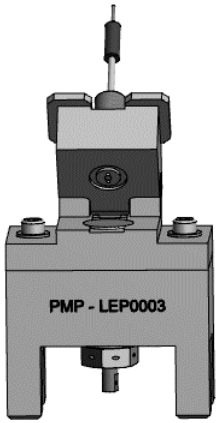

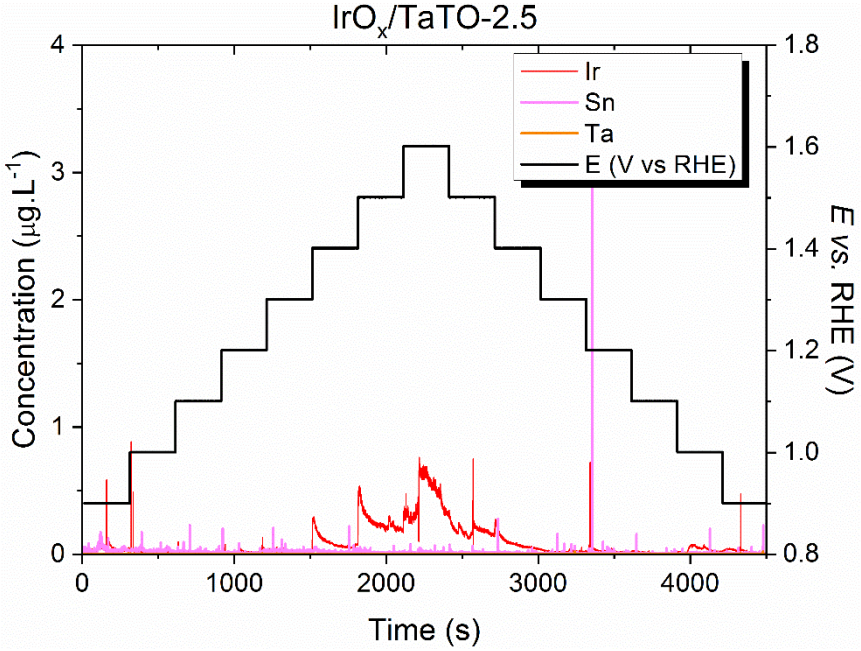

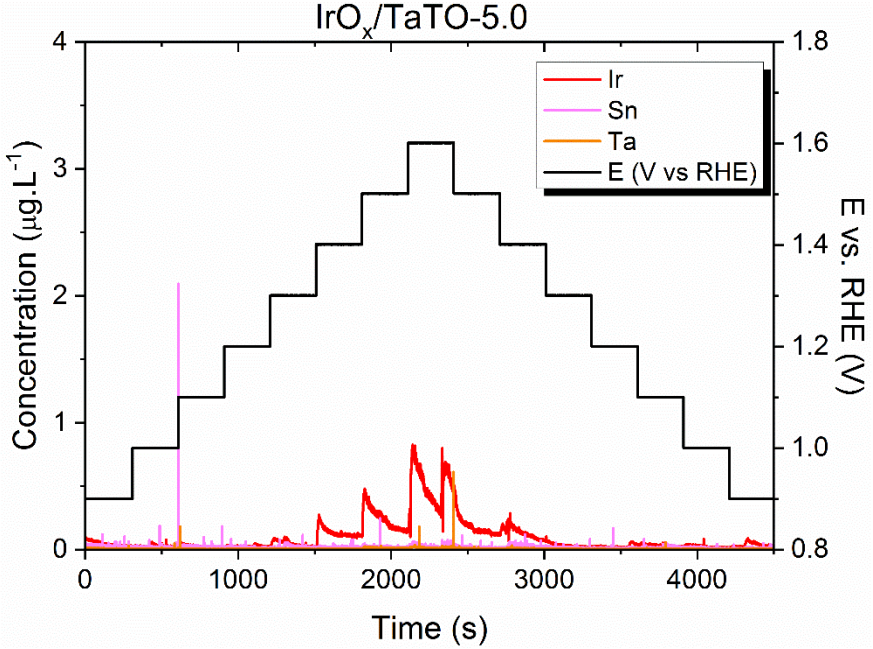

- ❑ Negligible Ta and Sn dissolution [1];
- ❑ Ir NPs dissolve at E > 1.4 V *vs*. RHE (similar to bulk Ir disk [2]).

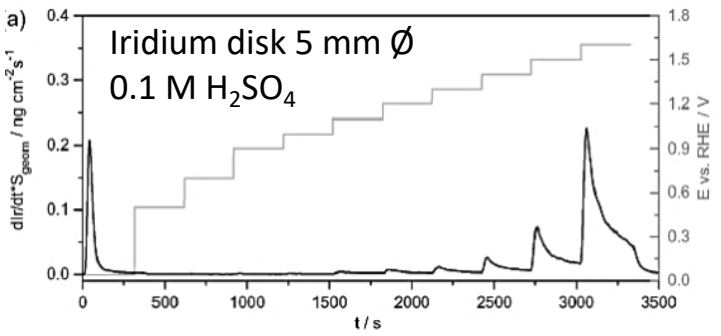

[1] S. Abbou, R. Chattot, V. Martin, F. Claudel, L. Solà-Hernández, C. Beauger, L. Dubau, F. Maillard, *ACS Catal.*, **2020**, *10*, 7283-7284.

[2] S. Cherevko, S. Geiger, O. Kasian, A. Mingers, K.J.J. Mayrhofer, *J. Electroanal. Chem.*, **2016**, *773*, 69–78

Spontaneous TaTO-core@Ta_2O_5-shell structure formation in acidic OER conditions

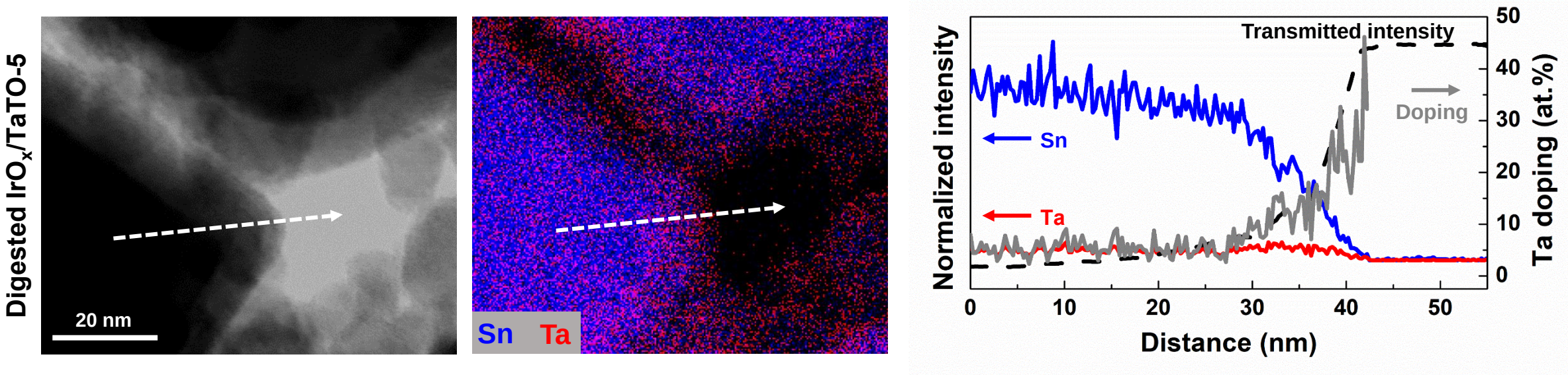

- Negligible Ta dissolution but formation of Ta_2O_5-shell [1].

[1] S. Abbou, R. Chattot, V. Martin, F. Claudel, L. Solà-Hernández, C. Beauger, L. Dubau, F. Maillard, *ACS Catal.*, **2020**, *10*, 7283-7284.

S-number values [1]

❑ **Subtle effect of thermal annealing under air.**

❑ Best illustrated by porous IrO_x NPs.

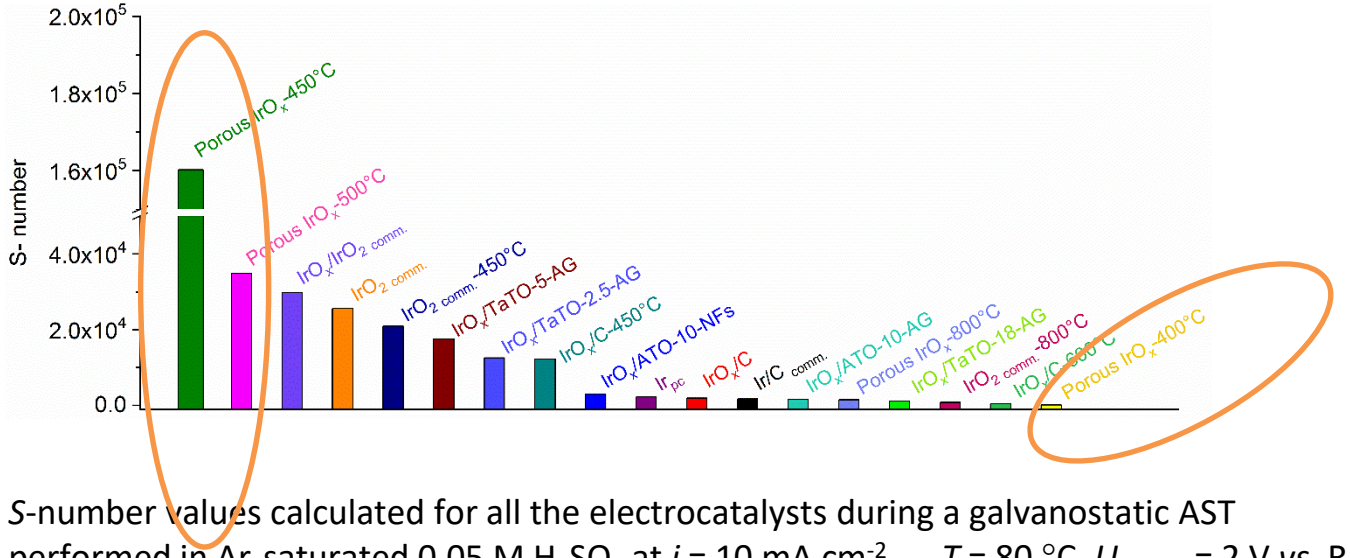

S-number values calculated for all the electrocatalysts during a galvanostatic AST performed in Ar-saturated 0.05 M H_2SO_4 at j = 10 mA cm^{-2}_{geo}, T = 80 °C, $U_{cut\text{-}off}$ = 2 V *vs.* RHE

$$\boldsymbol{S-number = \frac{n(O2)}{n(Ir)} = \frac{i}{i_{dissol}}}\ [1] \qquad n_{O_2} = \frac{1}{zF}\int i\,(t)dt \qquad n_{Ir} = \frac{[Ir]V}{M_{Ir}}$$

[1] Geiger, S.; Kasian, O.; Ledendecker, M.; Pizzutilo, E.; Mingers, A. M.; Fu, W. T.; Diaz-Morales, O.; Li, Z.; Oellers, T.; Fruchter, L.; Ludwig, A.; Mayrhofer, K. J. J.; Koper, M. T. M.; Cherevko, S., *Nat. Catal.* **2018,** *1* (7), 508-515.
[2] S. Abbou, R. Chattot, V. Martin, F. Claudel, L. Solà-Hernández, C. Beauger, L. Dubau, F. Maillard, *ACS Catal.*, **2020**, *10*, 7283-7284.

Effect of thermal annealing on structure and morphology of porous IrO_x NPs

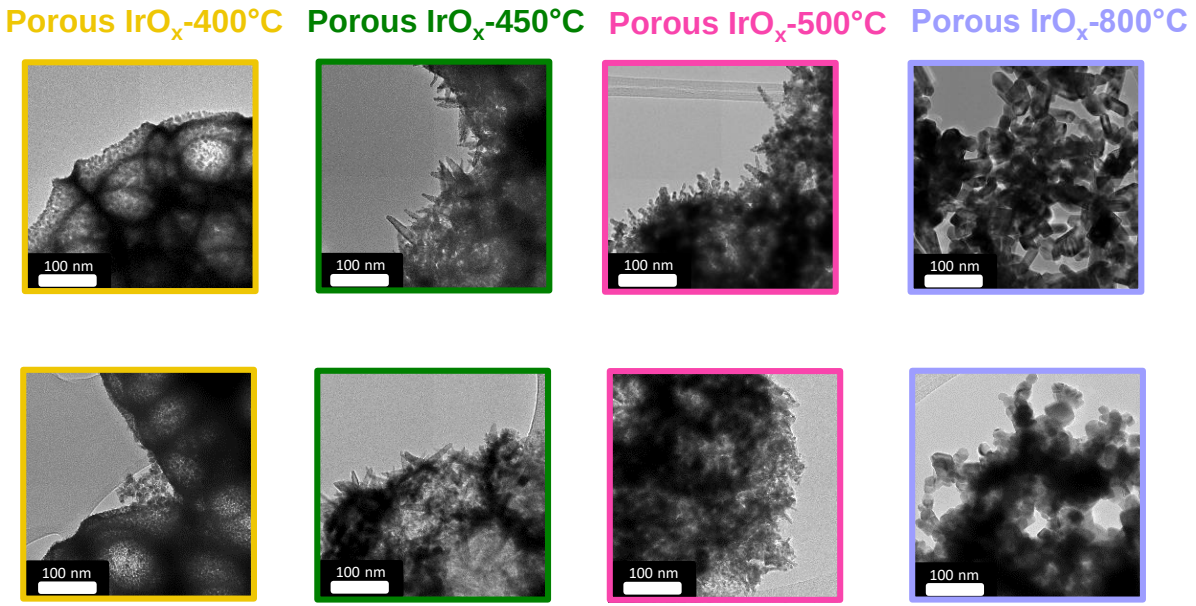

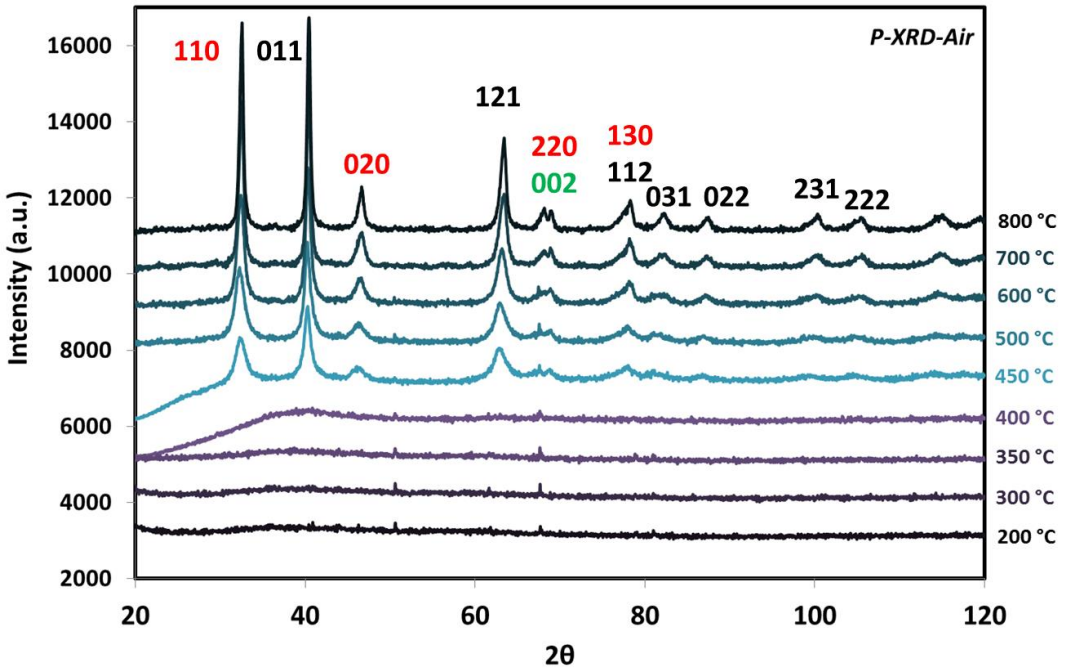

❑ **Subtle effect of thermal annealing under air.**

❑ At high *T*, increase of crystallite size and formation of Ir(+IV) species along with structure collapse.

Faustini, M.; Giraud, M.; Jones, D.; Rozière, J.; Dupont, M.; Porter, T. R.; Nowak, S.; Bahri, M.; Ersen, O.; Sanchez, C.; Boissière, C.; Tard, C.; Peron, J., *Adv. Energy Mater*. **2018**, 0, 1802136.

S-number values [1]

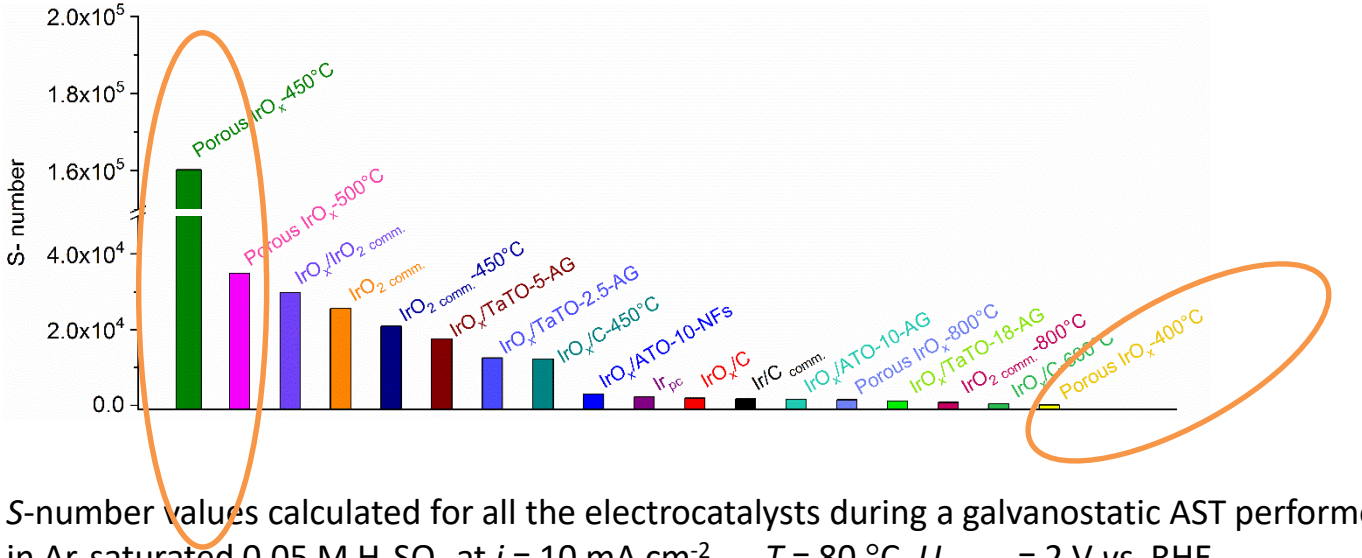

S-number values calculated for all the electrocatalysts during a galvanostatic AST performed in Ar-saturated 0.05 M H_2SO_4 at j = 10 mA cm^{-2}_{geo}, T = 80 °C, $U_{cut\text{-}off}$ = 2 V *vs.* RHE

❑ **Subtle effect of thermal annealing under air (see porous IrO_x NPS).**

❑ Thermal annealing at 450 °C causes recrystallization + formation of Ir(+IV) species: decrease of i_{dissol} → *S*-number increase,

❑ Thermal annealing at > 450°C leads to increase in crystallite size and structure collapse: decreased ASD values → smaller *i* values → *S*-number decrease

❑ Best compromise: Porous IrO_x-450°C

$$S - \text{number} = \frac{n(O2)}{n(Ir)} = \frac{i}{i_{dissol}} \text{ [1]}$$

$$n_{O_2} = \frac{1}{zF}\int i\,(t)dt$$

$$n_{Ir} = \frac{[Ir]V}{M_{Ir}}$$

[1] Geiger, S.; Kasian, O.; Ledendecker, M.; Pizzutilo, E.; Mingers, A. M.; Fu, W. T.; Diaz-Morales, O.; Li, Z.; Oellers, T.; Fruchter, L.; Ludwig, A.; Mayrhofer, K. J. J.; Koper, M. T. M.; Cherevko, S., *Nat. Catal.* **2018,** *1* (7), 508-515.
[2] S. Abbou, R. Chattot, V. Martin, F. Claudel, L. Solà-Hernández, C. Beauger, L. Dubau, F. Maillard, *ACS Catal.*, **2020**, *10*, 7283-7284.

Conclusions

❑ Library of 18 supported and unsupported materials:

- OER mass activity basis: Supported nanocatalysts > unsupported catalysts (high density of active sites because of amorphous domains/small crystallites + mixed Ir oxidation states);
- Long-term stability: Unsupported catalysts > supported catalysts;
- Long-term stability of supports: TaTO >> ATO ~ C;

❑ Thermal annealing under air enhances stability but lowers OER mass activity of IrO_x NPs (ASD + TOF decrease).

[1] F. Claudel, L. Dubau, G. Berthomé, L. Sola-Hernandez, C. Beauger, L. Piccolo, F. Maillard, *ACS Catal.*, **2019**, *9*, 4688-4698

[2] S. Abbou, R. Chattot, V. Martin, F. Claudel, L. Solà-Hernández, C. Beauger, L. Dubau, F. Maillard, *ACS Catal.*, **2020**, *10*, 7283-7284.

[3] C. Daiane Ferreira da Silva, F. Claudel, V. Martin, R. Chattot, S. Abbou, K. Kumar, I. Jiménez-Morales, S. Cavaliere, D. Jones, J. Rozière, L. Solà-Hernandez, C. Beauger, M. Faustini, J. Peron, B. Gilles, C. Beauger, L. Piccolo, F. H. Barros de Lima, L. Dubau, F. Maillard, *ACS Catal.*, **2021**, *11,* 4107-4116.

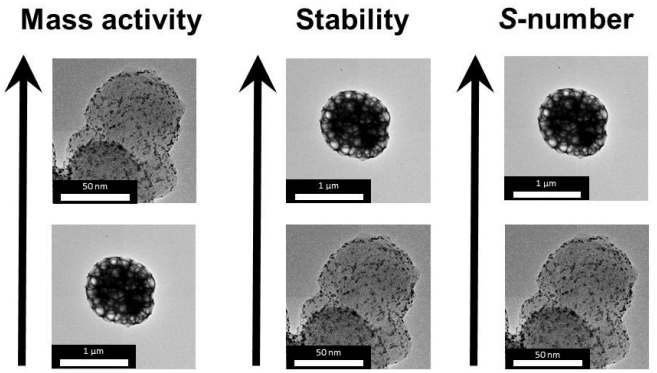

Synthesis of porous hollow IrO_x catalysts

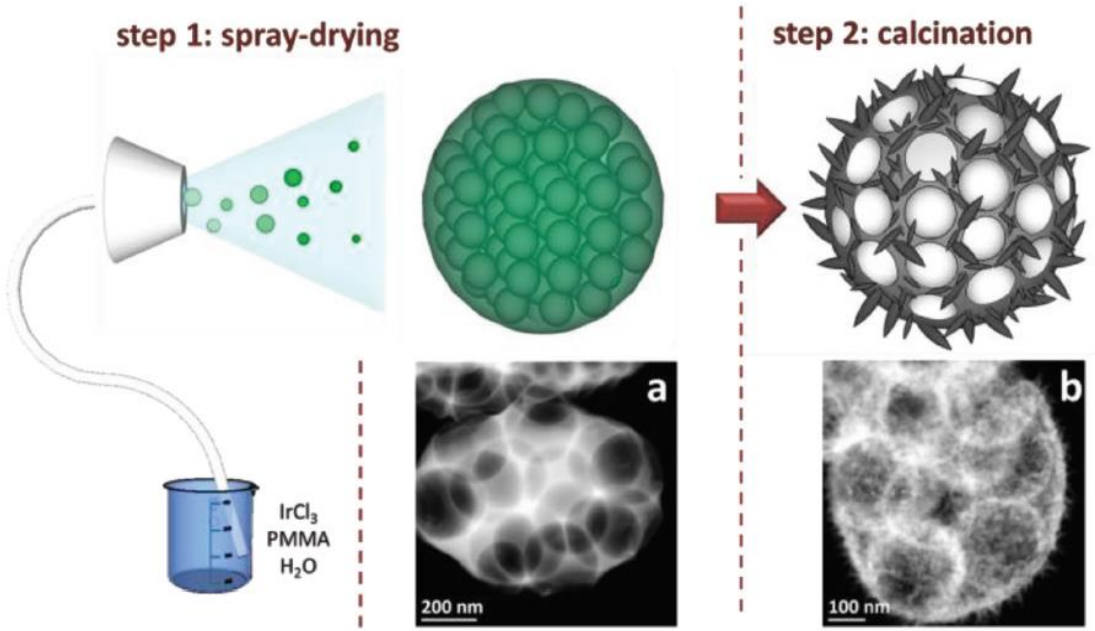

- $IrCl_3$ + PMMA solution sprayed → drying chamber → collection itnto glass vessel
- Calcination at different T leads to different crystallite sizes and change in Ir oxidation states

Porous IrO_x-400°C | Porous IrO_x-450°C | Porous IrO_x-500°C | Porous IrO_x-800°C

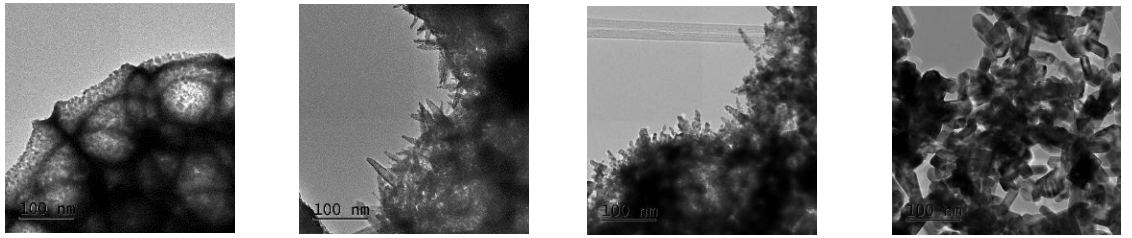

Faustini, M.; Giraud, M.; Jones, D.; Rozière, J.; Dupont, M.; Porter, T. R.; Nowak, S.; Bahri, M.; Ersen, O.; Sanchez, C.; Boissière, C.; Tard, C.; Peron, J., *Adv. Energy Mater*. **2018**, 0, 1802136.

Crystallite size rather than Ir oxidation state determines OER activity.

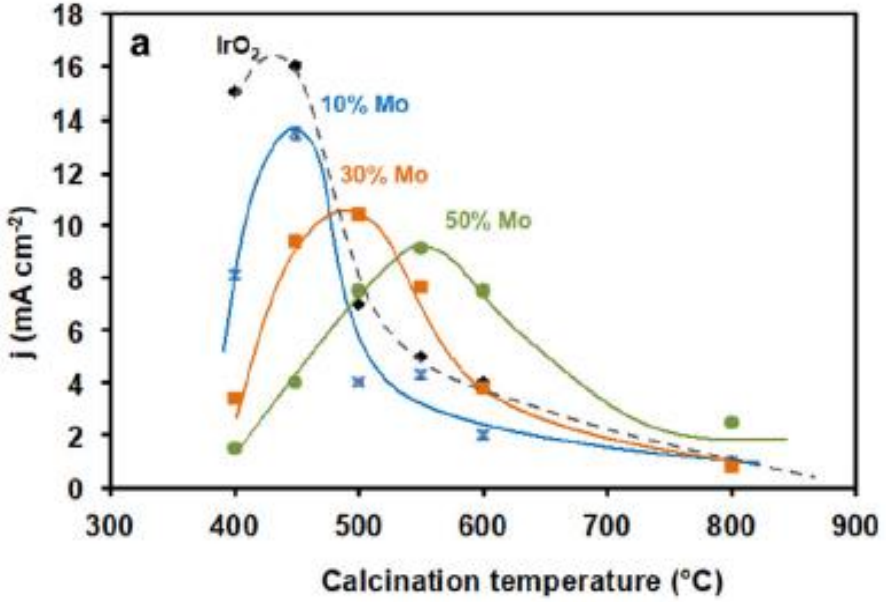

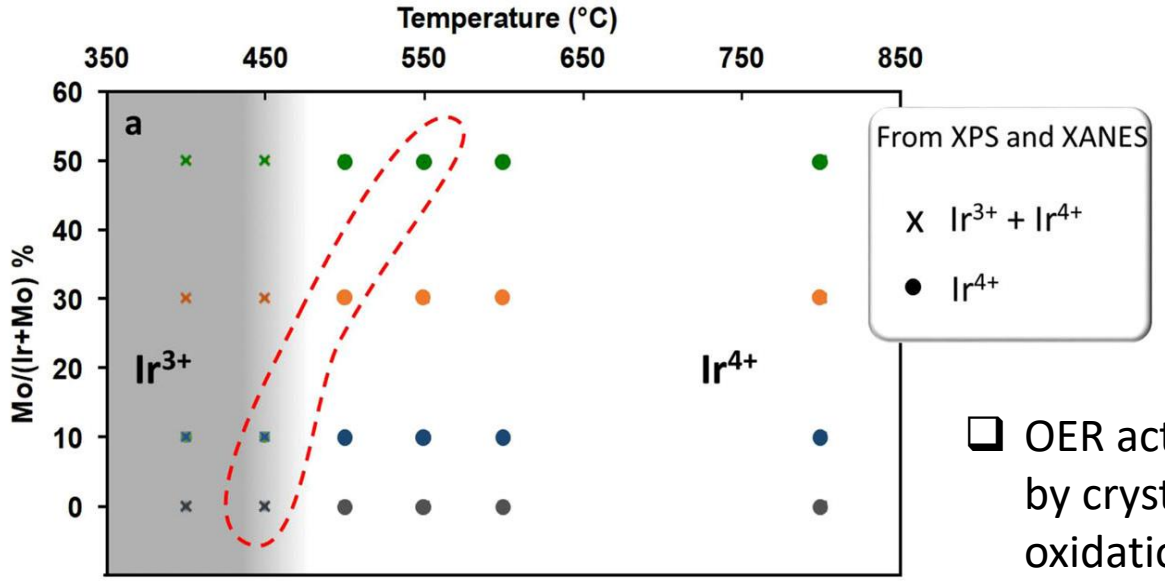

- OER activity governed by crystallite size, not Ir oxidation state.

[1] M. Elmaalouf, M. Odziomek, S. Duran, M. Gayrard, M. Bahri, C. Tard, A. Zitolo, B. Lassalle-Kaiser, J.-Y. Piquemal, O. Ersen, C. Boissière, C. Sanchez, M. Giraud, M. Faustini, J. Peron, *Nature Comm.*, **2021**, *12*, 3935.

Synthesis of doped SnO_2 aerogels

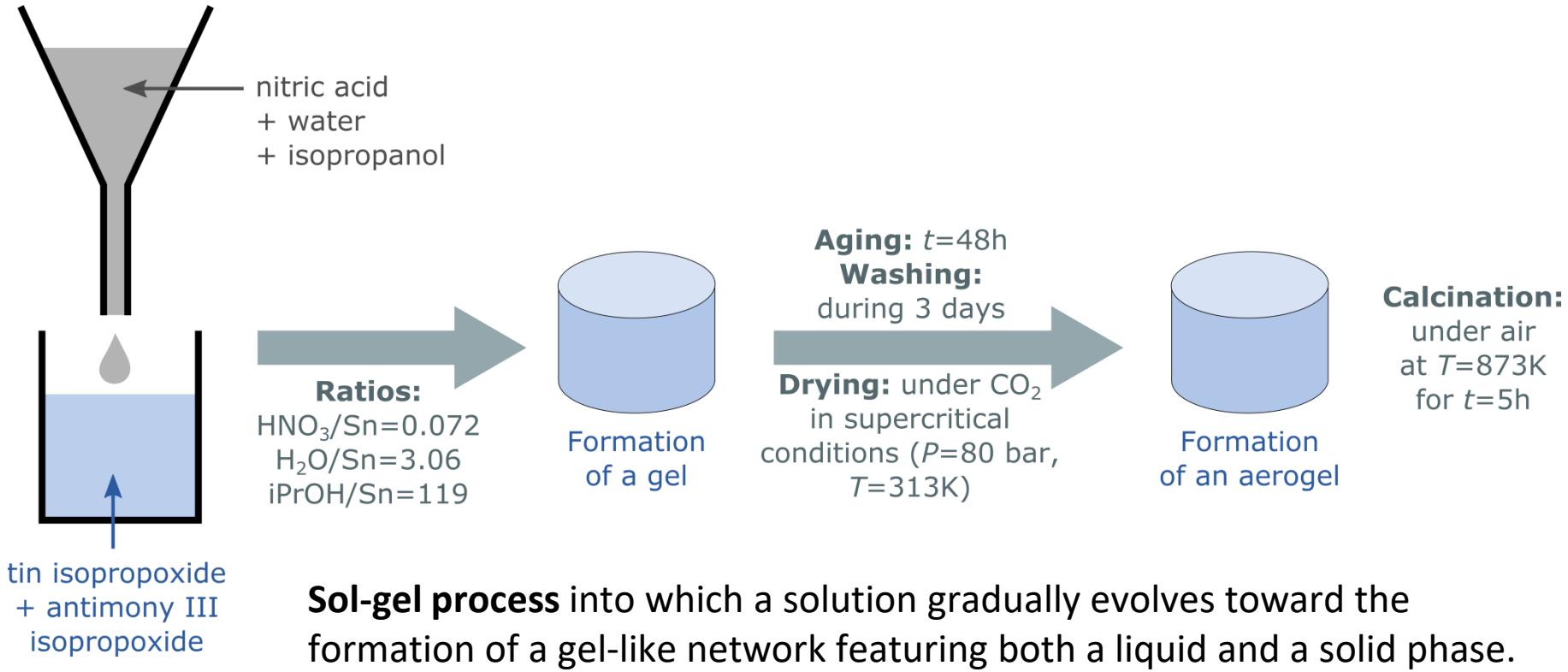

Sol-gel process into which a solution gradually evolves toward the formation of a gel-like network featuring both a liquid and a solid phase.

[1] Ozouf, G., Beauger, C., J. *Mater. Sci.,* **2016***, 51,* 5305-5320.
[2] L. Solà-Hernández, F. Claudel, F. Maillard, C. Beauger, *Int. J. Hydrogen Energy*. **2019**, 44, 24331-24341.

Sb-doped SnO_2 aerogels

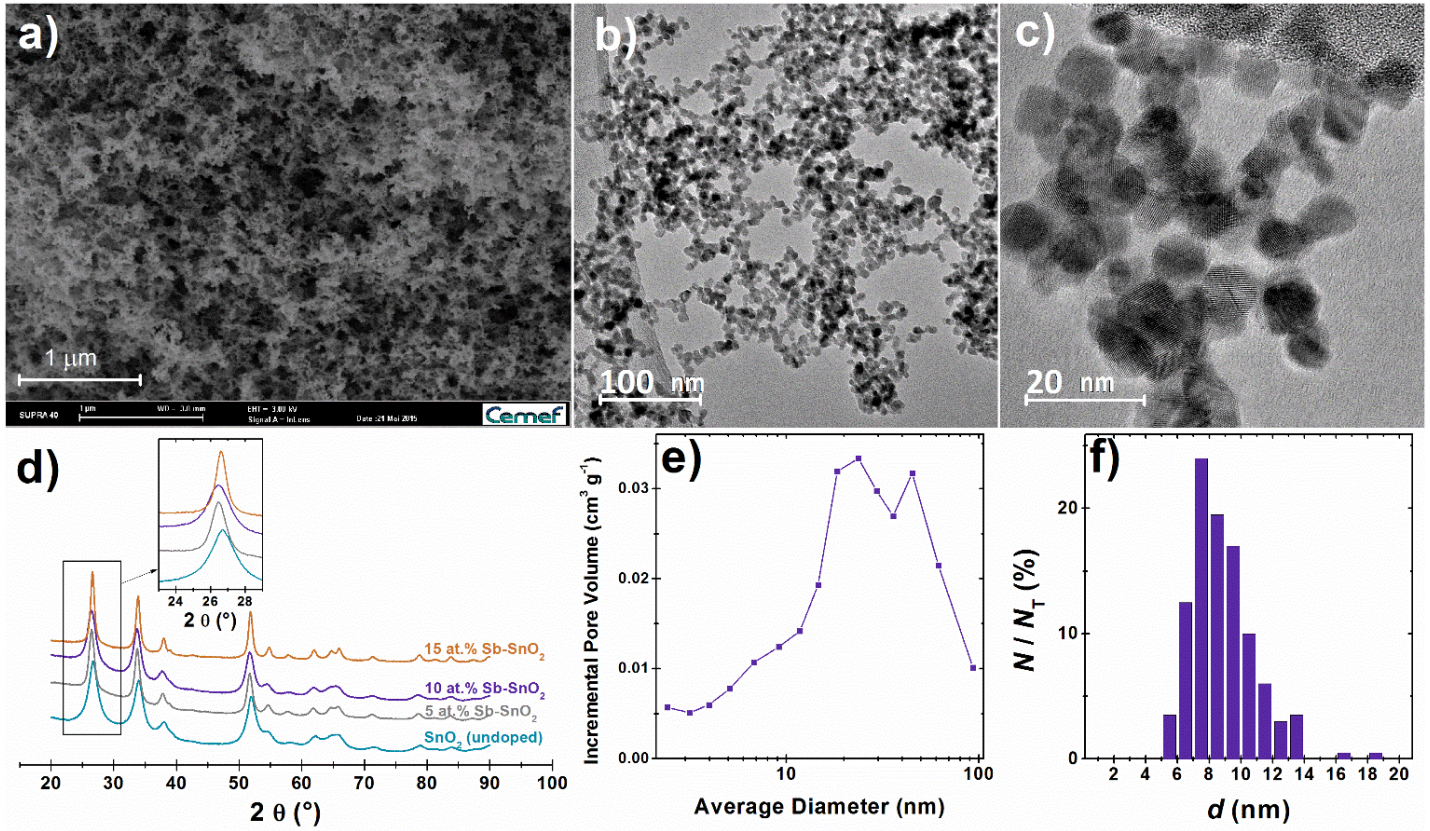

- ❑ Highly porous structure;
- ❑ High BET surface area (85 $m^2\ g^{-1}$), essentially 20-50 nm-sized pores (mesoporous);
- ❑ High electronic conductivity: 0.1 S cm^{-1}.

[1] Ozouf, G., Beauger, C., J. *Mater. Sci.,* **2016***, 51,* 5305-5320.
[2] L. Solà-Hernández, F. Claudel, F. Maillard, C. Beauger, *Int. J. Hydrogen Energy*. **2019**, 44, 24331-24341.

Structure of IrO_x catalysts

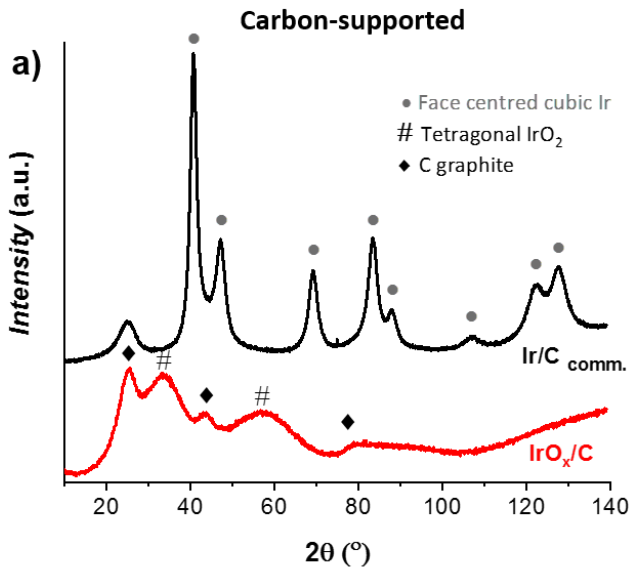

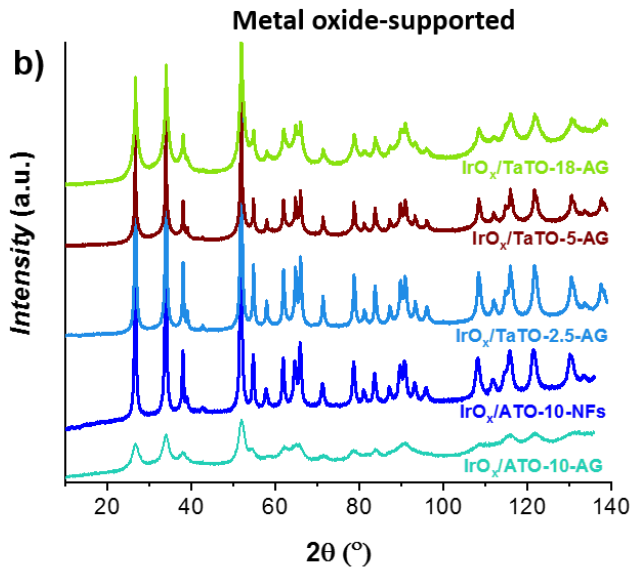

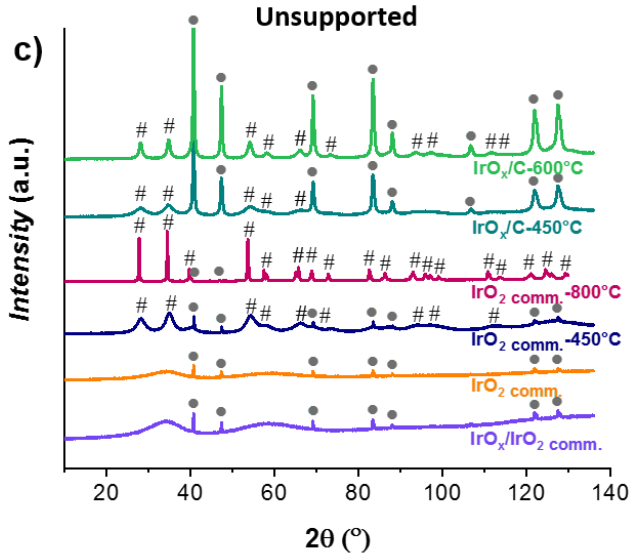

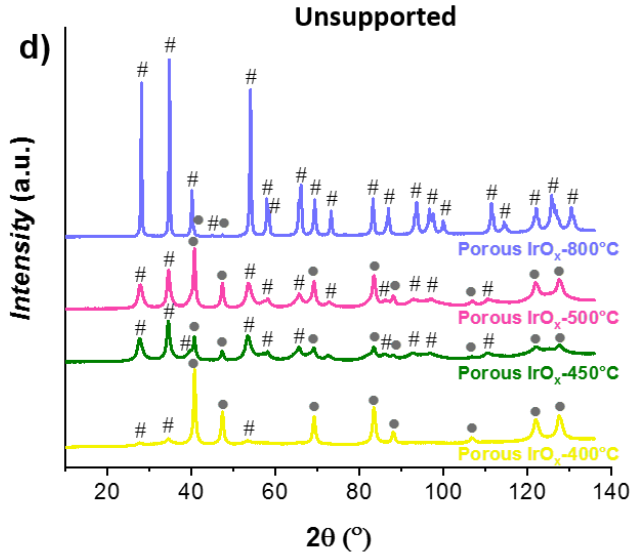

Chemical state of thermally-annealed IrO_x catalysts

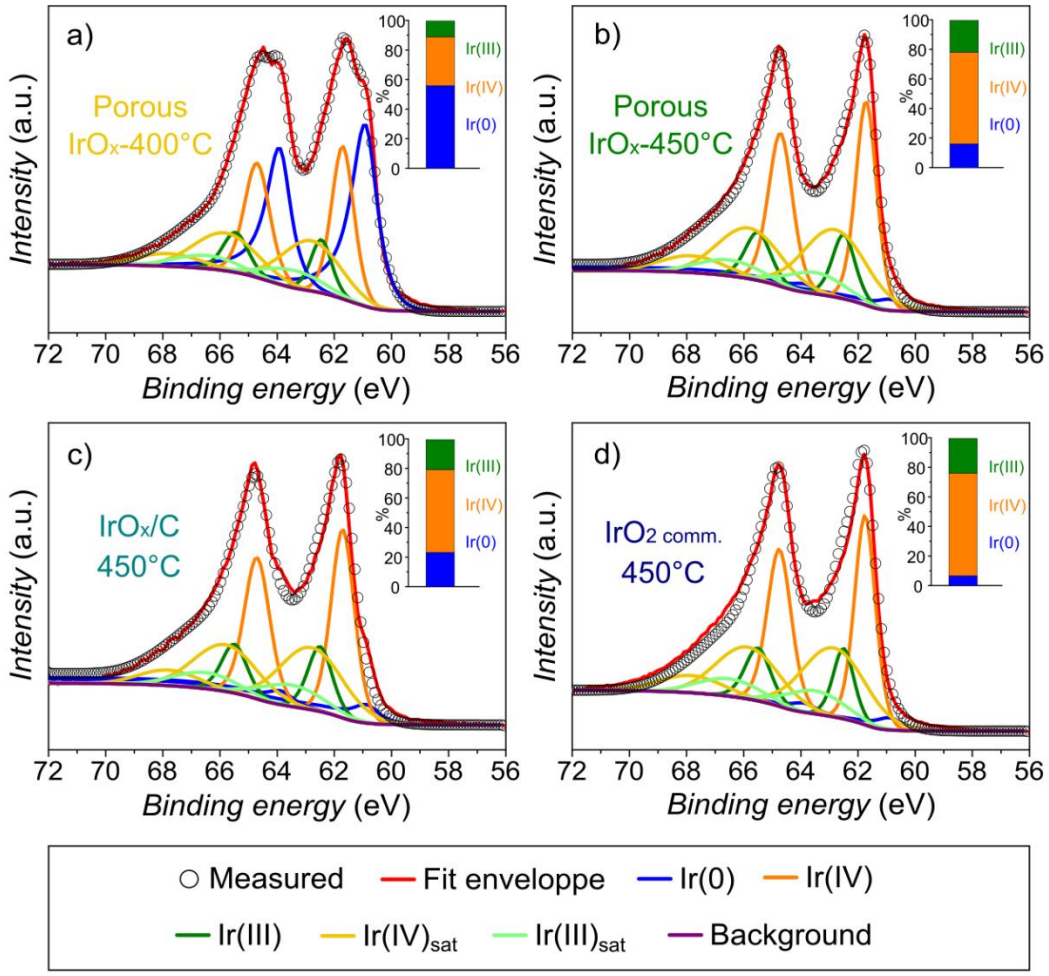

Effect of thermal annealing

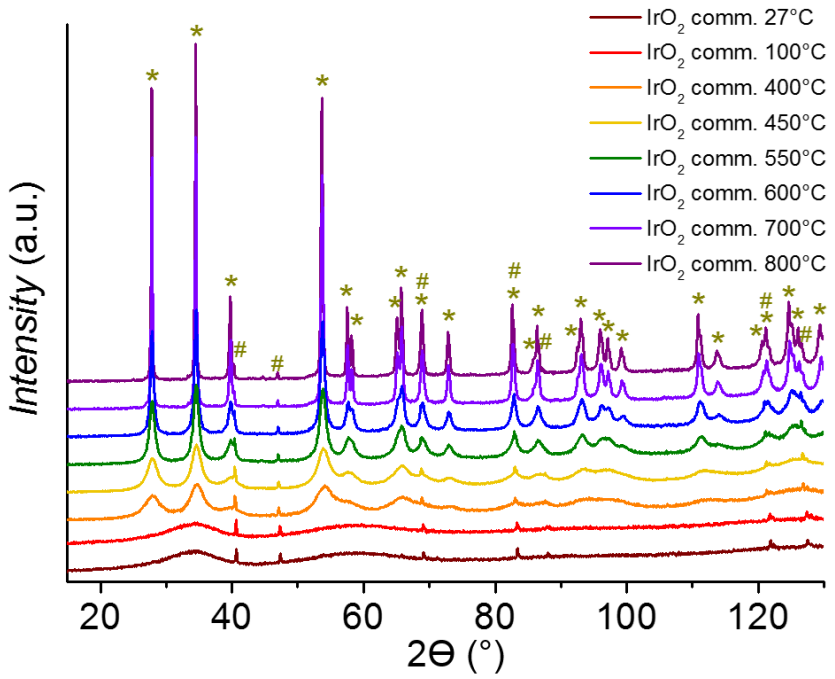

Electrochemical conditioning (10 cycles @ 10 mV/s between 0.9 – 1.4 V *vs*. RHE – 25°C)

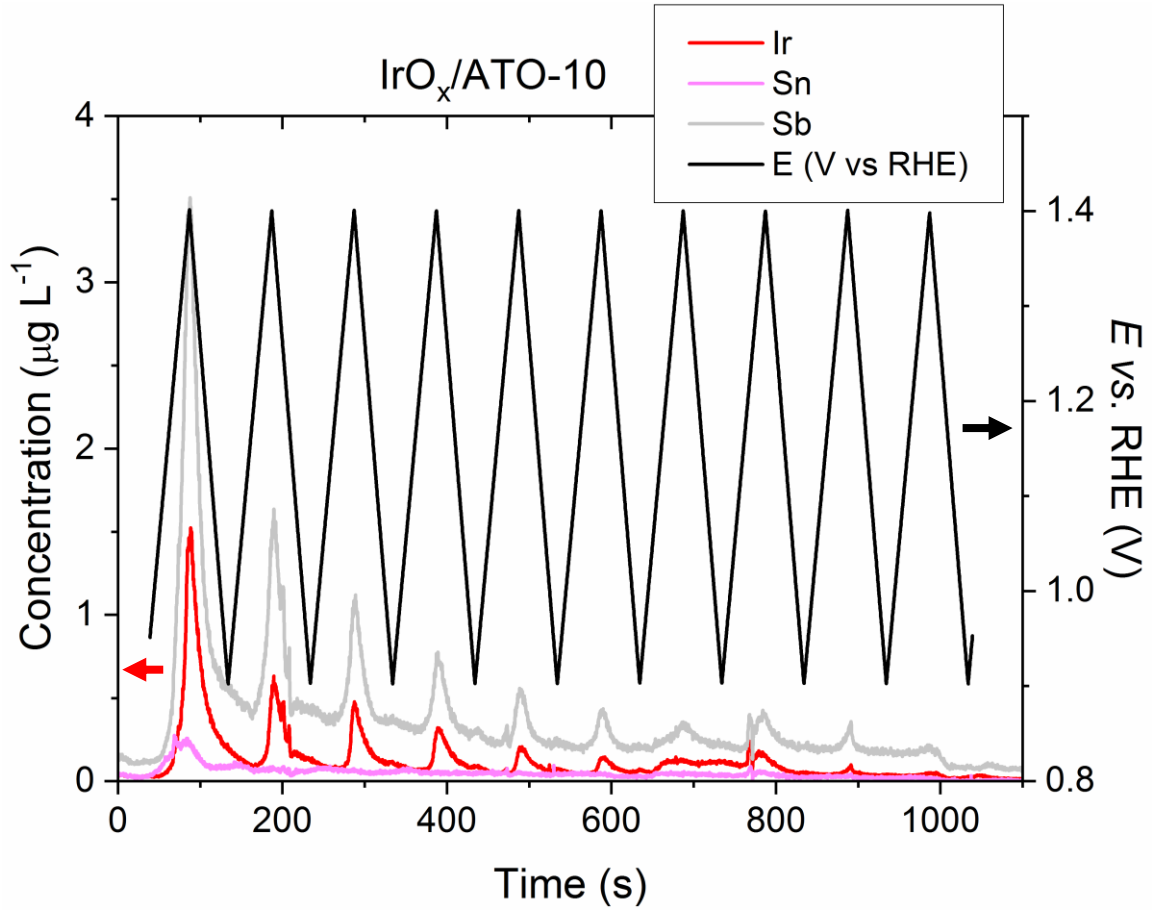

- Peaks originating from Ir and Sb;
- Decreasing quantities of Sb and Ir;
- Synchronous IrO_x and Sb peaks: detachment of portions of the catalytic layer?

Electrochemical conditioning

10 cycles @ 10 mV s^{-1}
[0.9 – 1.4 V *vs*. RHE]
25°C.

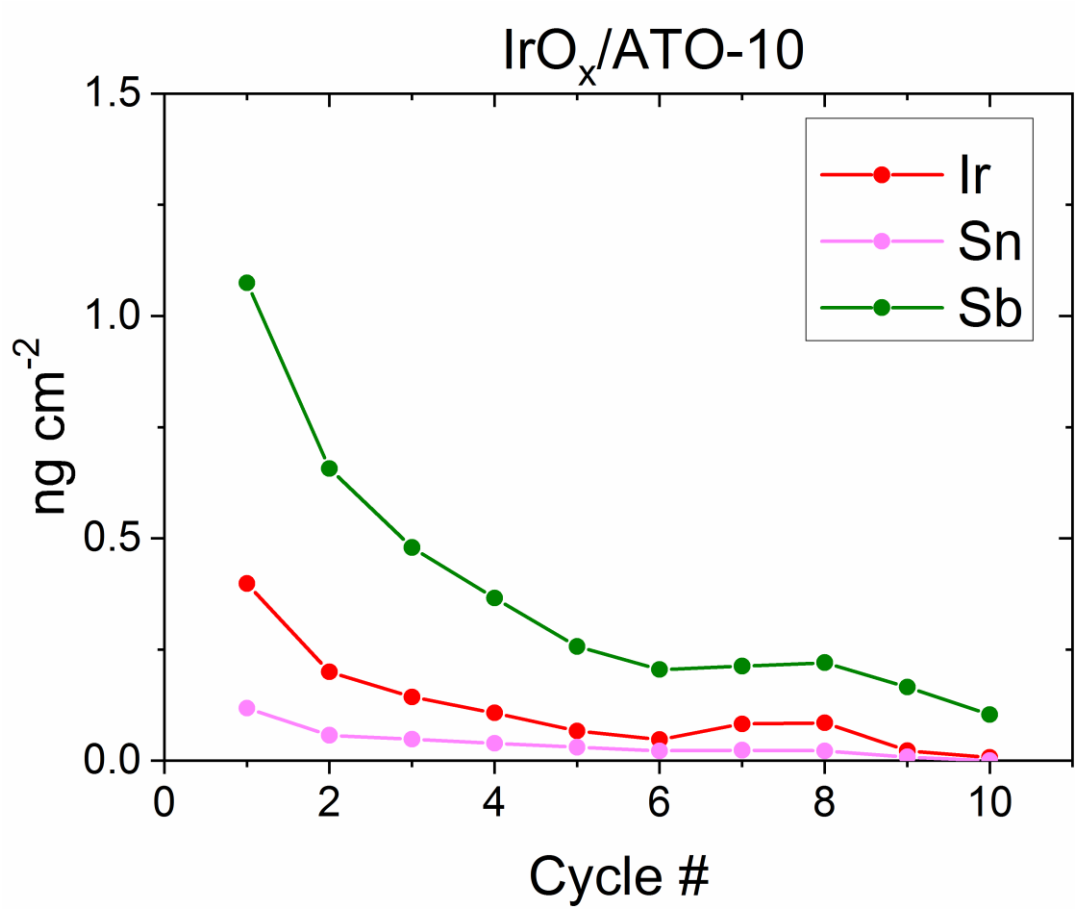

- Decreasing quantities of dissolved Sb and Sn;
- Synchronous IrO_x dissolution and Sb dissolution: detachment of portions of the catalytic layer due to oxygen evolution?

Electrochemical conditioning (10 cycles @ 10 mV/s between 0.9 – 1.4 V *vs*. RHE – 25°C)

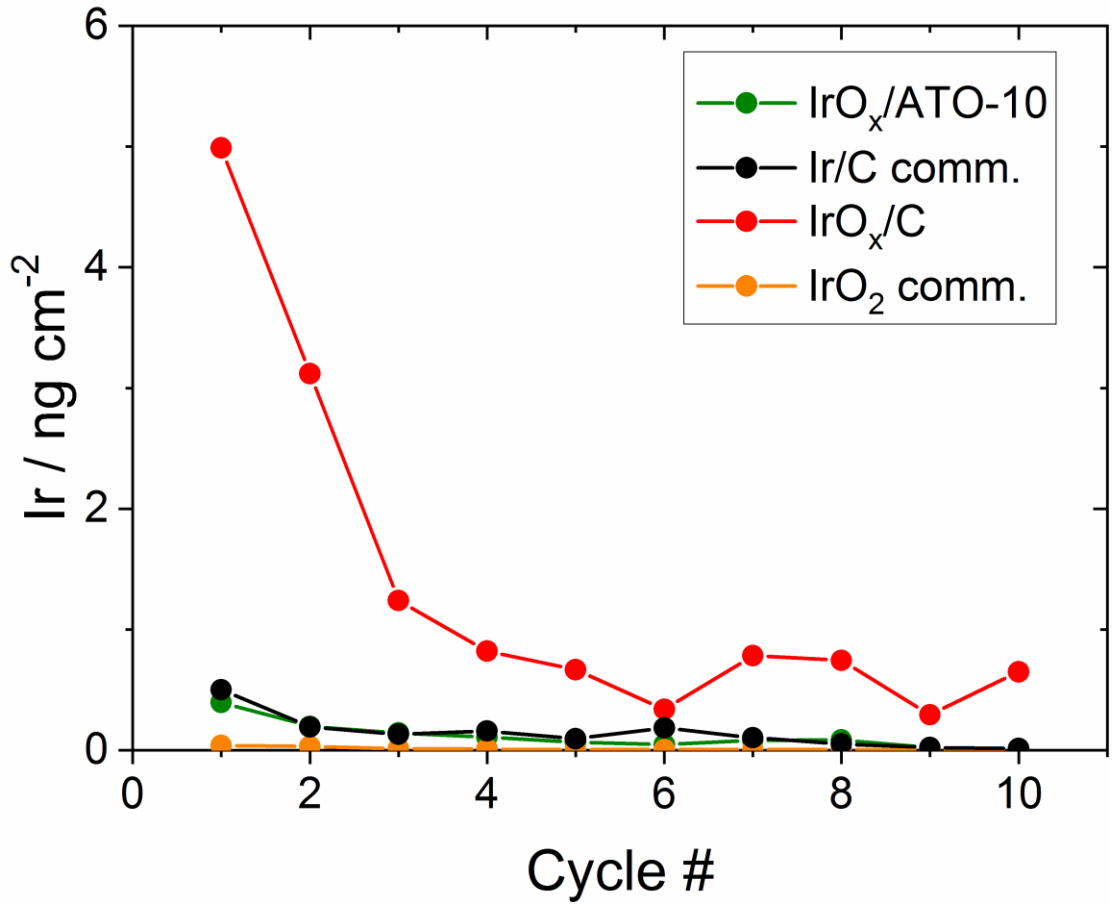

- IrO$_2$ comm. > Ir/C comm. ~ IrO$_x$/ATO > IrO$_x$/C
- Ir/C comm. more agglomerated than IrO$_x$/C

Electrochemical break-in

10 cycles @ 10 mV s^{-1}
[0.9 – 1.4 V *vs*. RHE]
25°C.

IrO_x/C

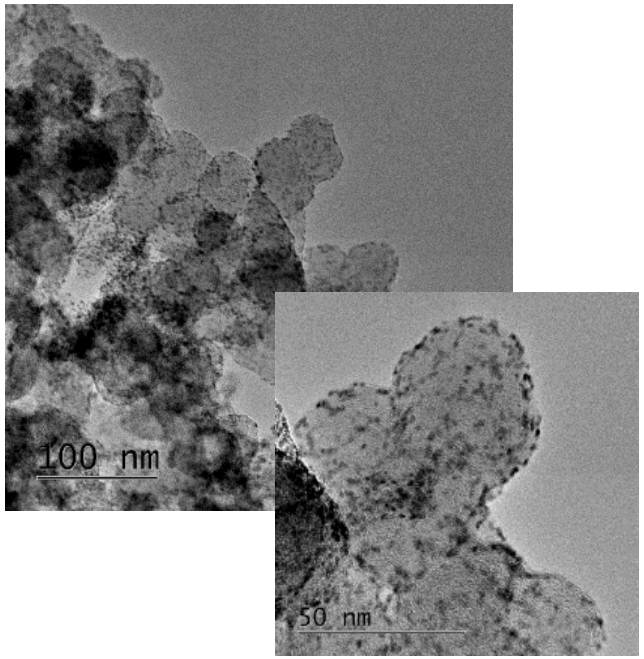

Ir/C comm.

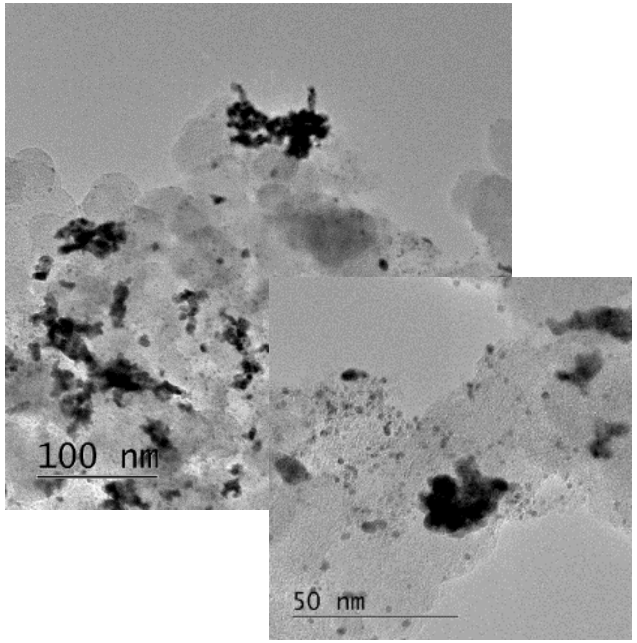

- IrO_2 comm. > Ir/C comm. ~ IrO_x/ATO > IrO_x/C
- Ir/C comm. more agglomerated than IrO_x/C

Electrochemical conditioning (10 cycles @ 10 mV/s between 0.9 – 1.4 V *vs*. RHE – 25°C)

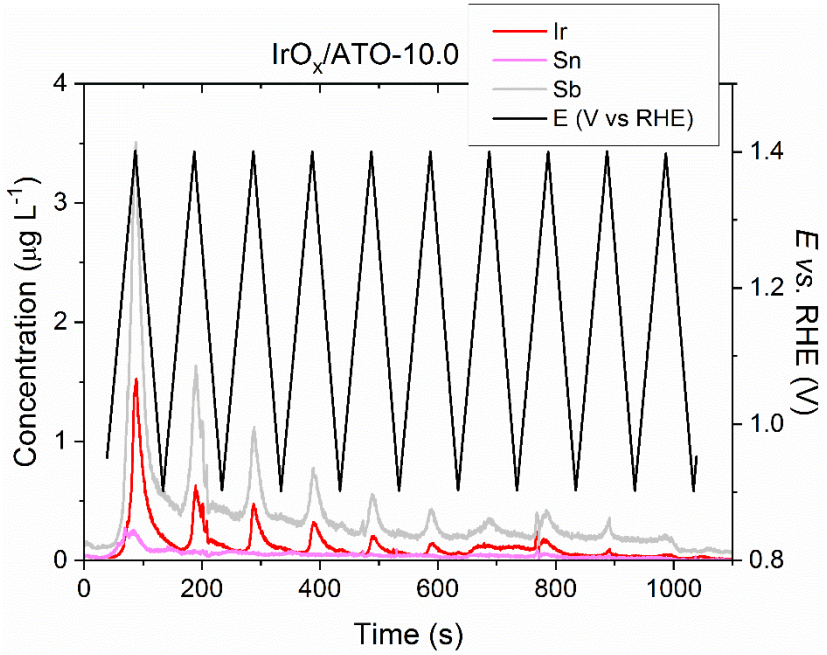

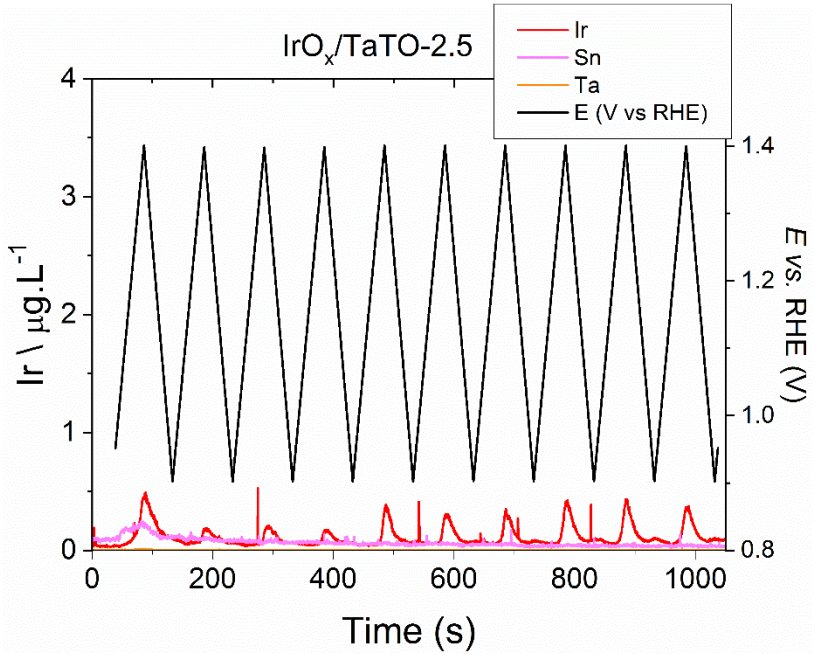

Electrochemical conditioning (10 cycles @ 10 mV/s between 0.9 – 1.4 V *vs*. RHE – 25°C)

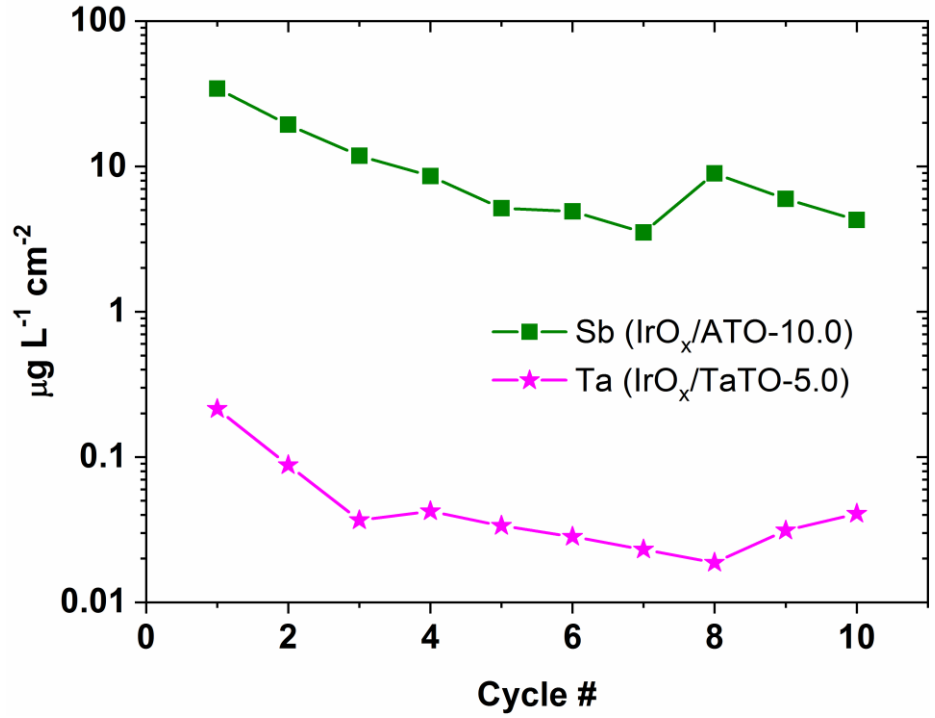

❑ Sb dissolution rate = Ta dissolution rate x 100 !

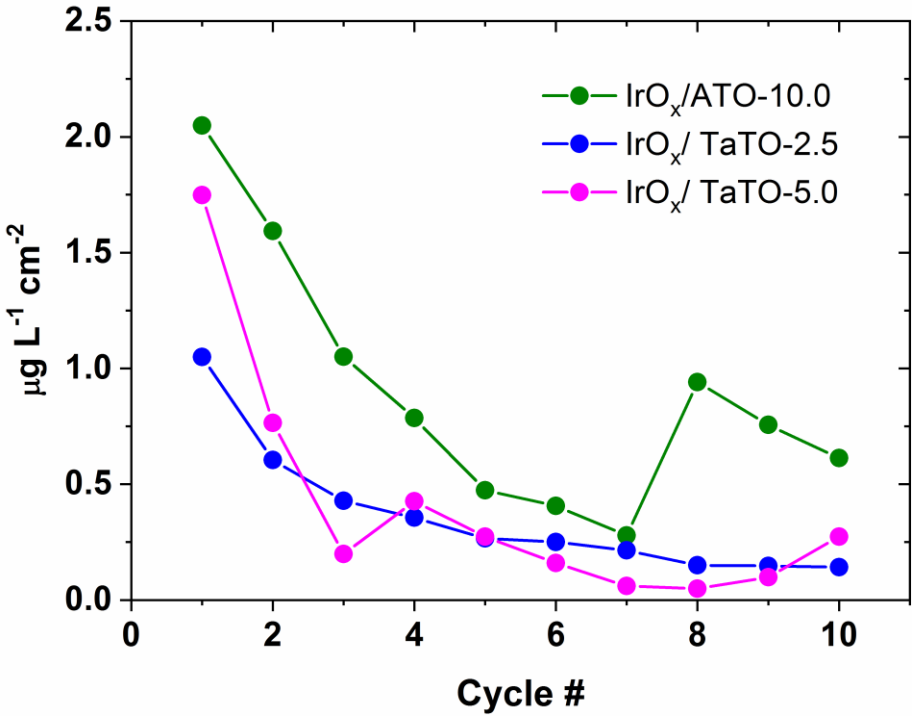

❑ Little effect of the dopant nature on the amount of detected Sn.

Electrochemical conditioning (10 cycles @ 10 mV/s between 0.9 – 1.4 V *vs*. RHE – 25°C)

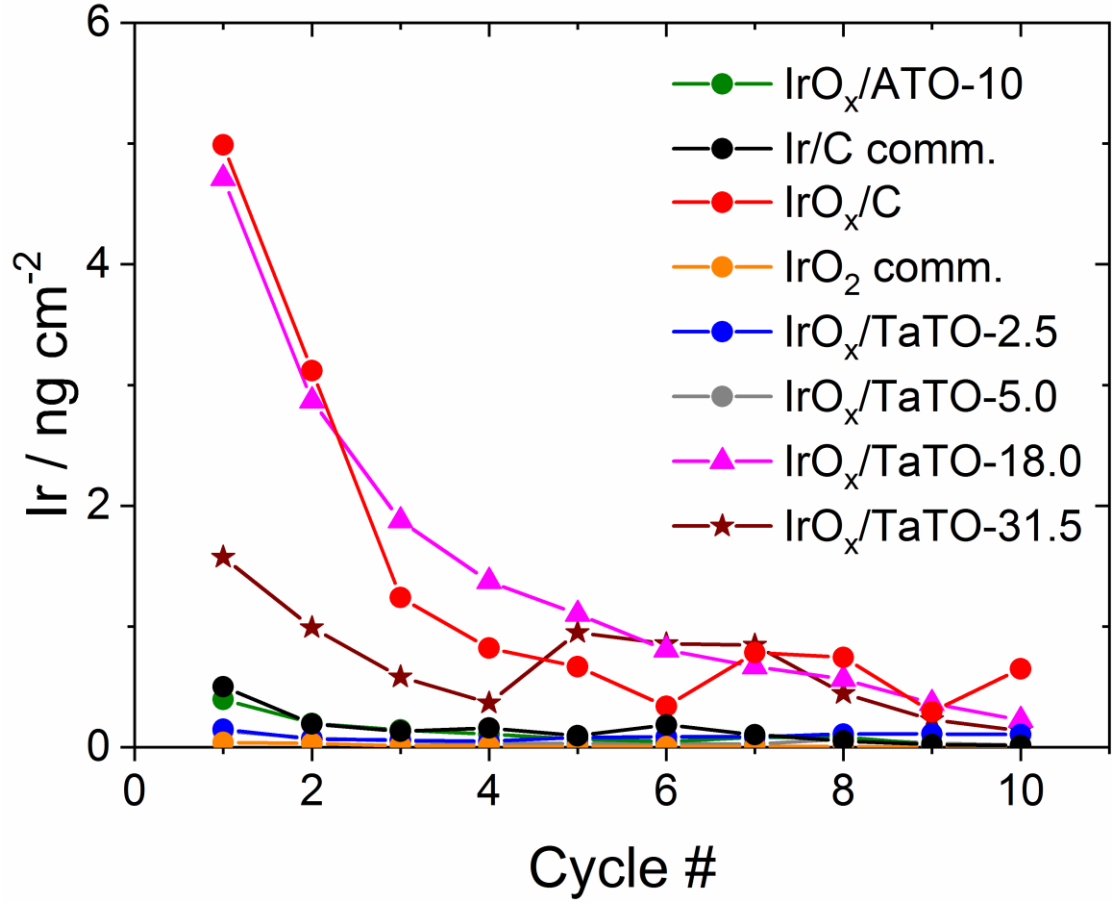

IrO_2 comm. > IrO_x/TaTO-2.5 ~ IrO_x/TaTO-5.0 > Ir/C comm. ~ IrO_x/ATO > IrO_x/TaTO-31.5 > IrO_x/TaTO-18.0 ~ IrO_x/C

Accelerated stress test (CVs between 1.2 – 1.6 V *vs*. RHE – 50 mV s^{-1} – 60°C)

- Enhanced CV stability for TaTO samples after cycling between 1.2 and 1.6 V *vs*. RHE @ 60 °C.

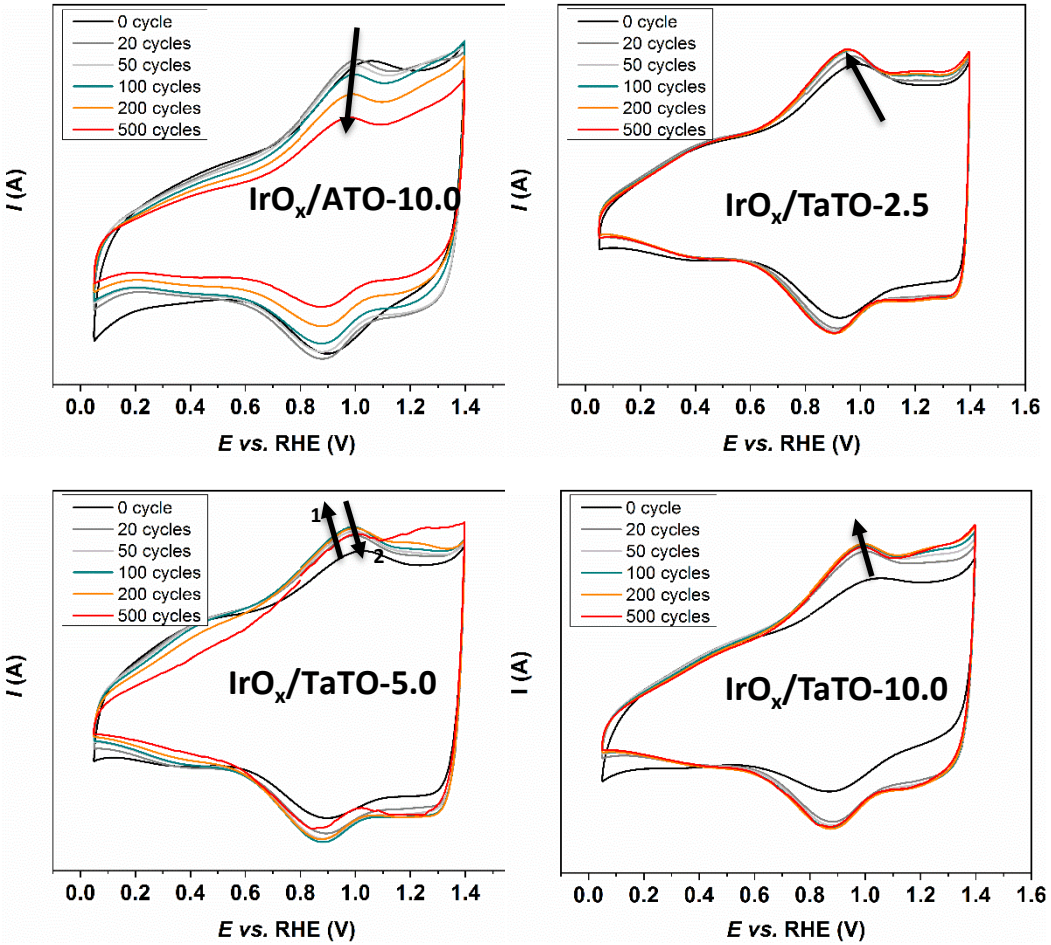

Accelerated stress test (CVs between 1.2 – 1.6 V *vs*. RHE – 50 mV s^{-1} – 60°C)

Activity @ 1.51 V *vs.* RHE after potential stepping between 1.2-1.6 V *vs.* RHE @ 60 °C

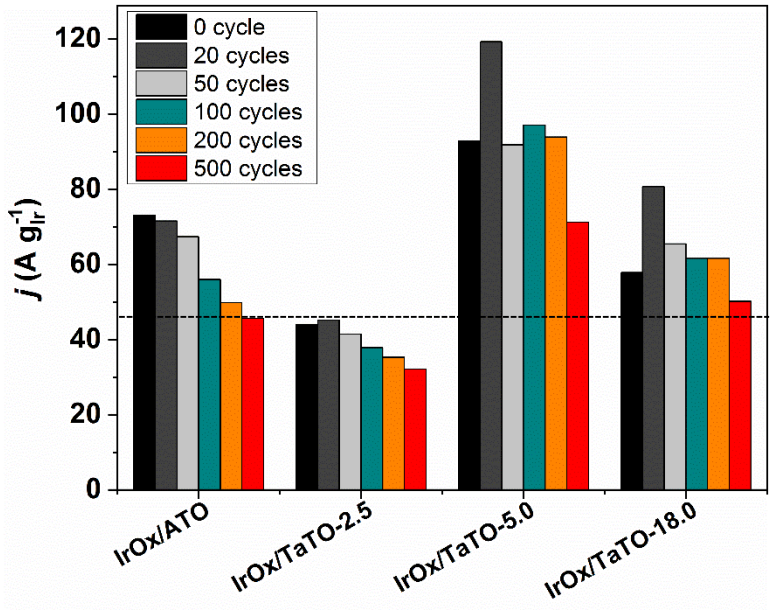

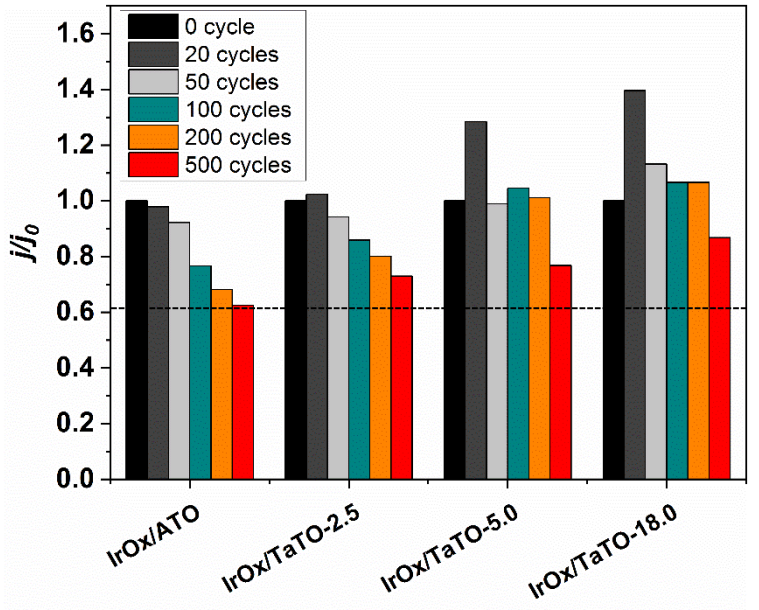

- Normalizing the OER current by the nominal Ir mass suggests superior activity and stability for IrO_x/TaTO 5 %;

- Increasing Ta content results in a better stability (up to 87 % of initial OER activity retained after 500 cycles between 1.2 and 1.6 V *vs*. RHE – *T* = 80°C).